Ore Geology Reviews 85 (2017) 271–298

Contents lists available at ScienceDirect

Ore Geology Reviews

journal homepage: www.elsevier.com/locate/oregeorev

The Vorontsovskoe Au-Hg-As ore deposit (Northern Urals, Russia): Geological setting, ore mineralogy, geochemistry, geochronology and genetic model

V.V. Murzin [a], E.A. Naumov [b,c,*], O.B. Azovskova [a], D.A. Varlamov [d], M.Yu. Rovnushkin [a], F. Pirajno [e]

[a] Zavaritsky Institute of Geology and Geochemistry of the UB RAS, 7 Pochtovy per, Yekaterinburg 620075, Russia
[b] V.S. Sobolev Institute of Geology and Mineralogy of the SB RAS, 3, Koptyuga prosp., Novosibirsk 630090, Russia
[c] Novosibirsk State University, 2, Pirogova st., Novosibirsk 630090, Russia
[d] Institute of Experimental Mineralogy RAS, 4, Acad. Osipian st., Chernogolovka, Russia
[e] Centre for Exploration Targeting, University of Western Australia, 35 Stirling Highway, Crawley, WA 6009, Australia

ARTICLE INFO

Article history:
Received 18 February 2016
Received in revised form 24 October 2016
Accepted 31 October 2016
Available online 4 November 2016

ABSTRACT

The large Vorontsovskoe Au-Hg-As deposit in the Urals is located in the exocontact of the Early Devonian Auerbah gabbro-diorite-granodiorite massif, which intrudes volcano-sedimentary rocks. The orebodies are confined to a tectonic contact of calcareous and tuffaceous rocks. They are composed of 6 types of disseminated ores, but the main reserves of gold are associated with the following ore types: gold-pyrite-arsenopyrite in altered tuffaceous rocks, pyrite-realgar ores in limestone breccia with a carbonate-volcanogenic cement, and gold-oxide-clay from regolith with residual gold. Early ore associations have been formed at 450–300 °C, whereas the late ores have been formed at lower temperature of 260–110 °C. We propose a model for the genesis of the Vorontsovskoe deposit based on synchronicity of mineralization with the formation of the Auerbah volcano-plutonic complex. The Ar-Ar age of hydromica from the gold-arsenopyrite association is 391.1 ± 4.9 Ma, which coincides with the age of igneous rocks of the Auerbah complex. The main sources of water and carbon dioxide were composed of the fluid derived from the magma chamber and the metamorphic water equilibrated with carbonate sedimentary rocks. Magmatic fluid dominated during the development of skarns, jasperoids and quartz veins, whereas metamorphic water was dominant during quartz-sericite alteration of volcano-sedimentary rocks and calcareous breccias. The bulk of the sulfur was supplied by a deep magma reservoir, however this source prevailed only during skarn ore formation. The mixing between deep-sourced sulfur and sedimentary or biogenic sulfur was established for other ore types. Gold and other ore components were possibly introduced during the volcanic and intrusive activity and also extracted from host sedimentary rocks.

1. Introduction

The Vorontsovskoe gold-mercury-arsenic deposit, discovered in 1985, is characterized by disseminated gold-sulfide mineralization in carbonate rocks. This mineralization, based on a number of geological, mineralogical, and geochemical features, was ascribed to the Carlin-style deposits. It is not surprising given that the Carlin-type gold-mercury-arsenic mineral system is one of the most important in the world, both in terms of gold reserves and the number of mined deposits. The specific features of the Carlin mineralization are: (i) confinement to the major thrust fronts within carbonate and siliceous-carbonate rocks (often carbonaceous), (ii) the presence of gold-sulfide mineralization represented by fine-grained sulfides with submicron or isomorphic gold, and (iii) gold-mercury-thallium-arsenic metal assemblages, associated with argillic and jasperoid alteration.

The major deposits of this type are located in the US (Carlin, Cortez, Getchell, Bell, Knoxville, etc.) (Radtke et al., 1980; Wallace, 1989; Sillitoe and Bonham, 1990; Berger and Bagbby, 1993; Ye et al., 2003; Emsbo et al., 2003; Cline and Hofstra, 2000; Hofstra and Cline, 2000; Cline et al., 2005; Nutt and Hofstra, 2003; Arehart and Donelick, 2006; Crafford and Grauch, 2002). They are also widely distributed in SE China in Shanxi, Guizhou and Hunan provinces (Shui, 1991; Cromie and Khin, 2003; Hu et al., 2002; Gu et al., 2002; Peters et al., 2007; Su et al., 2008, 2009; Maohong et al., 2011; Xia et al., 2012) and are known in other countries, such as Canada (Lefebure et al., 1998), Macedonia (Kochneva et al., 2006; Volkov et al., 2006a), Iran (Asadi et al., 1999, 2000; Mehrabi et al., 2003), Peru (Alvarez and Noble, 1988), Turkey (Çolakoğlu et al., 2011), India (Hazarika et al., 2013),

* Corresponding author at: V.S. Sobolev Institute of Geology and Mineralogy of the SB RAS, 3, Koptyuga prosp., Novosibirsk 630090, Russia.
E-mail address: naumov@igm.sbras.ru (E.A. Naumov).

http://dx.doi.org/10.1016/j.oregeorev.2016.10.037
0169-1368/

Northern Vietnam (Borisenko et al., 2008), Ukraine (Artemenko and Artemenko, 2002), and Kazakhstan (Kuzmina et al., 2013; Kovalev et al., 2009).

In Russia, mineral systems that can be attributed to the Carlin-style are scarce, although this Carlin affiliation remains questionable. Some geologists described as "Carlin-type" a number of gold deposits in Siberia, such as Sukhoi Log (Large et al., 2009), Maiskoe, Nezhdaninskoe (Sidorov and Volkov, 1998; Volkov et al., 2006a,b) and Kyuchus (Chudnenko et al., 2015); in the Far East - the Dzheltulakskoe and Oktyabrsky ore fields (Stepanov, 2000; Gromakovsky and Stepanov, 1999); in Eastern Sayan - the Vodorazdelnoye (Airiyants et al., 2007); and in the Urals - the Vorontsovskoe (Sazonov et al., 1998; Murzin et al., 2010).

The Vorontsovskoe is a major deposit with economically viable reserves. Currently, the deposit is being operated by "Northern Urals Gold" mining company (subsidiary of "Polymetall") with the ore being extracted from two open-pit mines (the northern and southern). Ore reserves of the deposit are 0.9 Moz of gold (JORC, 2012), with an average grade of 2.7 ppm

2. Sample preparation and analytical methods

Samples for this study were collected from the exploratory drill core carried out in 1991–1996, as well as from the northern and southern parts of the currently operated open pit at a depth of 140 and 40 m, respectively.

2.1. EMPA analyses

The study of morphology and chemical composition of the surface of the individual mineral grains was carried at the Institute of Geology and Geochemistry of the UB RAS using scanning electron microscope JSM-6390LV, equipped with EDS microanalyzer. The surface of pyrite grains was also studied by Auger electron spectroscopy using spectrometer LAS-3000 (Riber, France). Auger spectra were recorded in differential form: dN(E)/dE. The study of the chemical composition of minerals in polished samples was performed in a wave mode using the X-ray spectral microanalyzers JXA-5 and Cameca SH100, as well as a scanning microscope Tescan VEGAII XMU, equipped with an energy dispersive spectrometry INCA Energy 450 and a spectrometer with wave dispersion Oxford INCA Wave 700. The trace element composition of the rocks, ores and mineral monofractions was determined by ICP-MS technique using mass spectrometer ELAN-9000 (Perkin Elmer).

2.2. Organic matter study

Detection of organic matter particles was carried out on polished specimens using an electron microscope (JSM-6390LV, JEOL) and luminoscope. To determine the levels and types of organic matter and the degree of their metamorphism, we applied thermoanalytical studies on the derivatograph Diamond TG/DTA (Perkin Elmer). The error in determining the weight changes was $\pm 0.1\%$; the error of temperature peaks in the DTA was ± 0.3 °C. The composition of bitumens was studied by IR and NMR spectroscopy (analysts O.V. Koryakova, M.I. Kodess, IOS UB RAS, Yekaterinburg). The extraction of bitumoids (analyst N.N. Guseva, VIMS, Moscow) was carried out in a Soxhlet chamber with hot chloroform on a water bath for 50 h. IR spectra of bitumen were recorded on a spectrometer "Nikolet 6700" of "Thermo electron corporation" (USA), in the range of 4000–400 cm^{-1}. NMR spectra were obtained on a DRX-400 spectrometer of "Bruker BioSpin" company (Germany).

2.3. Geothermobarometry and fluid inclusion study

To evaluate the thermodynamic and physicochemical conditions of ore formation, we used bicarbonate geothermobarometry (Talantsev, 1981) and thermometry, based on the compositions of coexisting pyrite, pyrrhotite, and arsenopyrite (Kretschmar and Scott, 1976; Tulmin and Barton, 1968; Sharp et al., 1985), as well as the distribution of cobalt between pyrite and pyrrhotite (Bezmen et al., 1975). The gas-liquid inclusions in carbonate were studied using thermocryometry on a Linkam THMSG-600 heating-freezing stage. The salt composition of hydrothermal solutions in the inclusions was assessed by the eutectic temperature (Borisenko, 1977). The concentration of salts was calculated by melting points of the last crystalline phases (Bodnar and Vityk, 1994).

2.4. Isotope analytical methods

Sulfur isotope composition of sulfides was determined using the technique developed by Grinenko (1962) in the Vernadsky Institute (Analyst L.N. Grinenko) and TsNIGRI (analyst S.G. Kryazhev). The uncertainty in $\delta^{34}S$ doesn't exceed 0.2‰.

Isotopic analysis of carbon, oxygen, and hydrogen was performed in the analytical center at the FEGI FEBRAS on mass spectrometer Finnigan MAT 252 (ThermoFisher™) using a dual inlet system (Analyst T.A. Velivetskaya). Preparation of carbonate samples for measurement of oxygen and carbon isotopic compositions was carried out following the method described by Velivetskaya et al. (2009), using 100% phosphoric acid. The reproducibility of measurements of $\delta^{18}O$ and $\delta^{13}C$ (1σ) is 0.1‰ and 0.05‰, respectively. Calibration of method was conducted according to in-house and international standards: NBS-18, NBS-19, and IAEA-CO-8. Quartz sample preparation for oxygen isotopic composition measurement was performed by the laser method (infrared laser MIR-10-30, New Wave Research, USA). Reproducibility of $\delta^{18}O$ values was 0.1‰ (1σ). The carbon isotopic composition of carbon dioxide, extracted from the gas-liquid inclusions, was measured with an accuracy of ± 0.15‰.

Water and carbon dioxide from the gas-liquid inclusions in quartz were recovered by heating the samples at T = 1000–1100 °C. Reproducibilities of isotopic composition for carbon dioxide and water were 0.15‰ (1σ) and 1.5‰ (n = 5), respectively. Calibration was carried out using the international standards VSMOW, SLAP and GISP.

The isotopic composition of strontium in carbonates was determined at the Institute of Geology and Geochemistry UB RAS (by Yu.L. Ronkin). Crashed carbonates (0.1–0.2 g) were decomposed into cold 3 N acetic acid for 2–24 h. Measurements were carried out using the TIMS Finnegan MAT-262. Reproducibility was controlled by parallel measurements MTI standard. The values of the measured $^{87}Sr/^{86}Sr$ ratio were normalized to $^{87}Sr/^{86}Sr = 0.1194$

$^{40}Ar/^{39}Ar$ dating of the sample K-hydromica was performed at the Institute of Geology and Mineralogy of Siberian branch of Russian Academy of Sciences (Novosibirsk) using mass spectrometer Micromass Noble gas 5400 (analyst A. Travin) by step heating technique in a quartz reactor. The errors correspond to the interval of $\pm 1\sigma$. Plateau age was calculated according to the age range method (Fleck et al., 1977).

3. Tectonic setting of the ore field

The Vorontsovskoe Au-Hg-As deposit is situated on the eastern slopes of the Northern Urals, 12 km south of the town Krasnoturyinsk. At the regional scale, it is located in the eastern part of the Tagil zone within the Auerbah volcano-plutonic belt of Lower-Middle-Devonian age (Fig. 1). According to modern concepts, this belt was formed in an active continental margin as a result of collision of the Tagil island arc with the eastern Urals microcontinent (Yazeva et al., 1988).

The rocks of the Auerbah volcano-plutonic belt form a tectonic depression (graben-syncline) about 35 km long and 18 km wide (Fig. 2). This structure is made up of volcanic and volcano-sedimentary rocks with lenses of limestones, which are combined into the Krasnoturinsk suite. The intrusive rocks of the Auerbah massif are comagmatic with

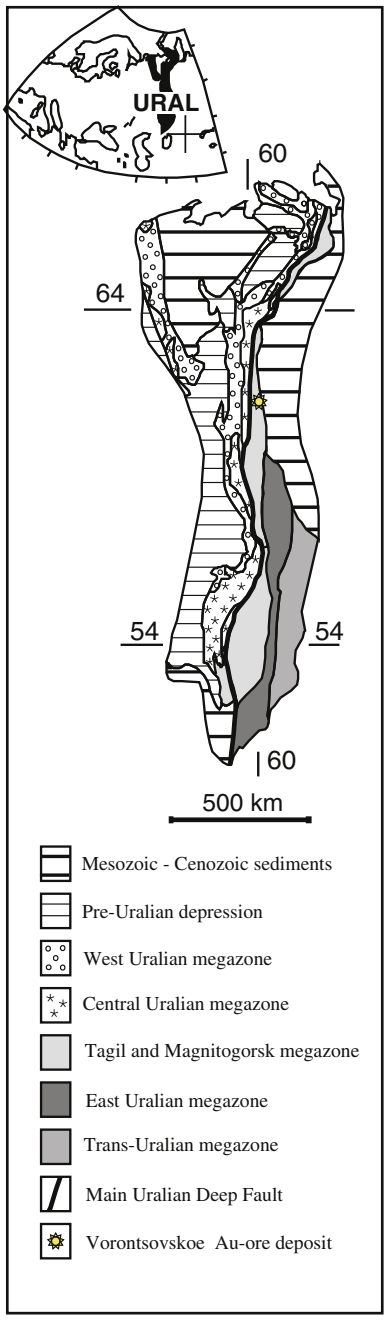

Fig. 1. Location of the Vorontsovskoe deposit in the Urals.

volcanic rocks and are represented by diorites, quartz diorites, and granodiorites.

The Vorontsovskoe deposit belongs to the Turinsk-Auerbah metallogenic province. Gold-skarn magnetite and magnetite-copper deposits, as well as quartz vein-hosted gold deposits, occur within the contact zone between carbonate rocks of the Krasnoturyinsk suites and the Auerbah intrusion. These deposits are likely to be the source of numerous gold placers of various ages (from mid-late Jurassic to Quaternary).

4. Geology of the Vorontsovskoe Au-Hg-As deposit

The Vorontsovskoe deposit is located along the southwestern exocontact of the Auerbah gabbro-diorite-granodiorite intrusion (Fig. 3). It is confined to the limb of a monoclinal structure gently dipping to the west and composed of volcano-sedimentary rocks of the Krasnoturyinsk suite. This suite is divided into three units or series. The Lower Frolov-Vasilyev unit (up to 1200 m thick) is composed of gray, light gray organogenic-clastic marmorized limestones with thin interbedded tuffaceous sandstones and tuffaceous siltstones. On the contact with the intrusion, the limestones are marmorized; hornfels haloes are also well developed. The overlying volcano-sedimentary rocks of Bashmakov series (up to 150 m thick), with a distinct unconformity, are represented by thinly interbedded tuffites (siliceous, calcareous), tuffaceous sandstones, andesite and andesite-basalt tuffs. The Bogoslov series (up to 220 m thick) overlying the Bashmakov unit is established on the northern and southern flanks of the deposit; it is made up of crystal-tuffs, agglomerates of andesite and andesite basalts, siliceous tuffaceous sandstones with lenses of limestone, and lavas of plagioclase andesites.

The Krasnoturyinsk sedimentary rocks are intruded by numerous dikes, mostly of intermediate-mafic composition, from dolerites and gabbro-dolerites to diorite- and quartz-diorite porphyries and lamprophyres. Most dikes are represented by propylitized, in places skarn-altered diorite porphyries. Propylitized dikes carry disseminated sulfides, mainly pyrite. Skarn-altered dikes along contacts are accompanied by magnetite-sulfide mineralization. Minor lamprophyres also contain disseminated pyrite. Most of the dikes are considered to be pre-ore with respect to the Au-Hg-As mineralization (Sazonov et al., 1991). The gold content in the dikes does not exceed 0.2 ppm (Nechkin and Rovnushkin, 2011).

The mineralization is controlled by three structural factors: 1) horizon marker of the contact between the Frolov-Vasiliev limestones and Bashmakov volcanic sequence; 2) slightly inclined thrusts and associated crash zones, and 3) steeply dipping to the west faults, some of which control the mafic and intermediate dikes (Fig. 3).

In the contact zone, there is a brecciated limestone horizon of unclear origin, hosting a major part of the ore bodies. Fragments of breccia are represented by limestones, in places marmorized and recrystallized, whereas cement is composed of a mixture of volcanic material with carbonate. The origin of brecciated limestones is not clear. There are few hypotheses that attempt to account for their formation, such as eruptive, tectonic, sedimentary and volcanic-sedimentary. The first hypothesis is that the eruptive breccias were formed by volcanic material filling the voids during simultaneous volcanism and tectonic crush of limestone (Sazonov et al., 1991). The tectonic hypothesis suggests that breccias were formed during crushing and marmorization of limestones due to the Auerbah intrusion (Rakhov, 1999). According to the sedimentary and volcano-sedimentary hypotheses, breccias, along with tuffaceous sandstone and tuffaceous siltstone layers, were accumulated in depressions on the surface of the collapsed reef structures (Minina, 1994; Cheremisin and Zlotnik-Khotkevich, 1997).

Altered rocks, accompanied by elevated concentration of gold, commonly occur within the deposit and comprise: skarns, propylites, listvenites, quartz-sericite rocks, jasperoids and argillic rocks (Sazonov et al., 1998). In addition, recent studies have established the overprinting character of carbonaceous alteration (bituminization), which is shown in some rock types (Azovskova et al., 2013a).

The formation of regolith material and karst has occurred in the Early-Middle Mezosoic (Sigov, 1969). This is confirmed by the presence of deluvial-proluvial and lacustrine-alluvial deposits of Middle-Late Jurassic age of the Langursk suite, containing placer gold.

5. Ore types

The ore-bearing zone is a submeridionally elongated band (Fig. 4). More than 48 ore zones have been recognized and explored. However, more than 90% of reserves are concentrated in four main orebodies, exploited in the northern and southern open-pit workings. The orebodies are composed of three types of ores (A, B and C), among which we identified six mineral types (Table 1). All economically important ore types have similar distribution of gold contents. The gold

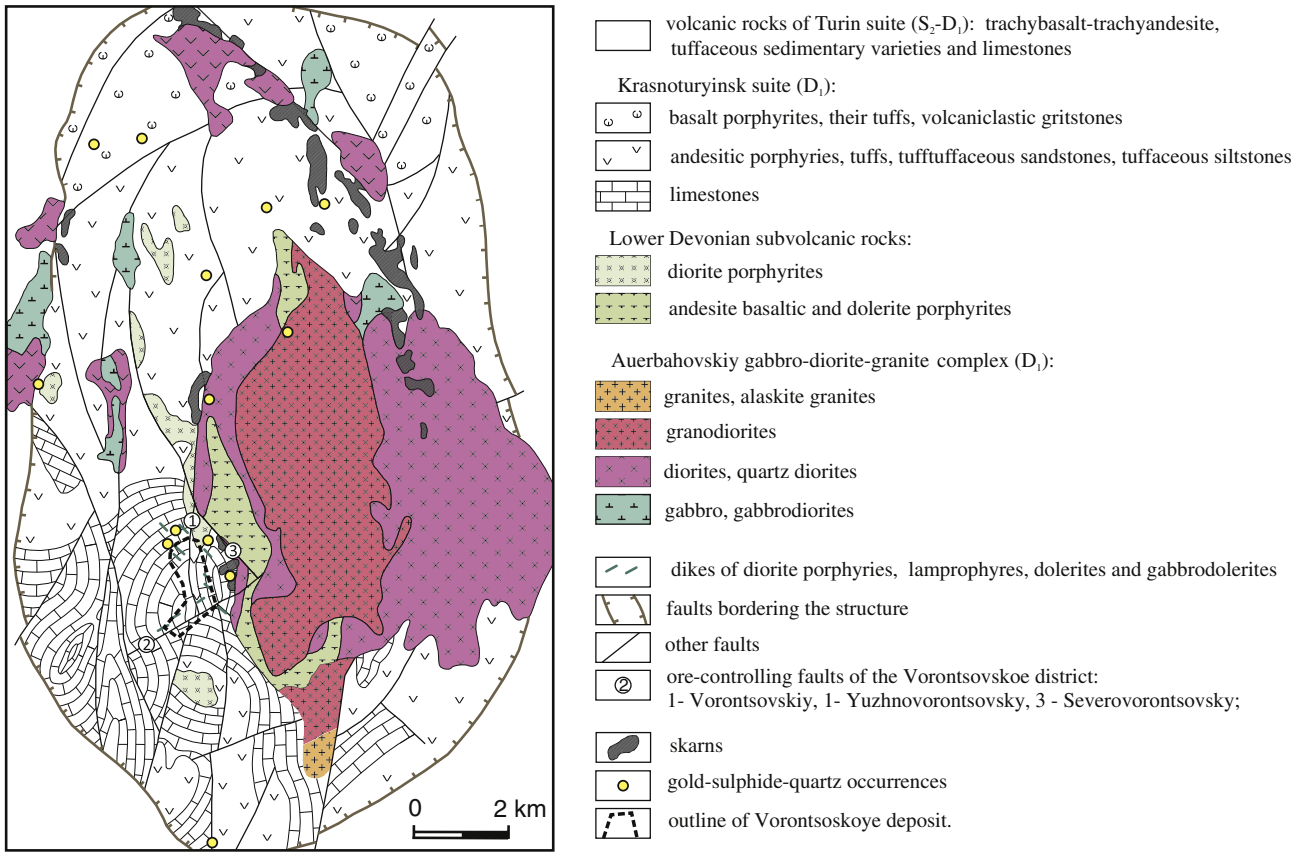

Fig. 2. A schematic geological map of the Turinsk-Auerbah ore district.
After Rindzyunskaya et al. (1995).

content in 66–87% of samples is less than 5 ppm Au, whereas in 84–94% of samples its amount is lower than 10 ppm.

5.1. Type A1. Disseminated gold-magnetite-sulfide ores in calcareous skarns

Gold-bearing magnetite-sulfide ores in garnet, pyroxene-garnet, and epidote skarns are minor at the Vorontsovskoe deposit and they occur mainly on its northern and southern flanks. Skarns are confined to the contacts of small diorite intrusions and/or the intermediate and mafic dikes and form interbeds in the tuffaceous rocks. They are common in endocontacts of the Auerbah intrusion, which has a number of well-documented magnetite deposits, such as Vorontsovskaya and Peschanskaya (Korzhinskiy, 1948; Ovchinnikov, 1948; in 1960, etc.). Skarn ores containing up to 6.2 ppm Au are represented by infill of magnetite and up to 10 vol.% sulfides (pyrite, pyrrhotite, chalcopyrite, sphalerite, galena). Calculations of mass balance of gold (Grigor'ev et al., 1992) showed that at the bulk Au content of 0.01 ppm, about 50% is contained in sulfides. When the bulk Au content is 1 ppm, it is concentrated in the form of native metal.

Away from the ore zone, rare bodies of gold-bearing wollastonite skarns of small thickness occur among limestones, containing infills of silver-polymetallic mineralization represented by arsenopyrite, pyrite, pyrrhotite, chalcopyrite, sphalerite, galena, pyrargyrite, and Ag tellurides (Sazonov et al., 1991). Another rare type of gold-bearing skarn is found in the endo- and exocontact zones of a small diorite body on the southern flank of the deposit. These skarns of garnet-epidote and calcite-epidote-garnet composition have disseminated chalcopyrite, bornite, Ag, Au, Hg tellurides (hessite, coloradoite, calaverite, altaite, tellur-bismuthite), and native gold (fineness up to 830–920).

5.2. Type A2. Disseminated jasperoid-hosted gold-polymetallic ores

The size of auriferous jasperoids ore bodies varies from a few tens of centimeters to 1–2 m thick and up to 10–15 m long. They are located mainly in the northern and southern margins of the main ore zone. The sulfide polymetallic mineralization is represented by thick disseminations (reaching up to the massive ore) of pyrite, sphalerite, chalcopyrite, galena, and fahlore in silicified tuff siltstones and limestones associated with jasperoidal quartz. The low-sulfide (up to 2–3 vol.% sulfides) sulfosalt-polymetallic mineralization is represented by scattered pyrite, arsenopyrite, sulfides, and Cu, Zn, and Pb sulfosalts. It occurs in brecciated limestones, tuffaceous siltstones, as well as in the dikes associated with the jasperoidal dolomite-ankerite. The geochemical association of the ores consists of Ag, Pb, Zn, Cu, Sb, and S. The Au/Ag ratio is essentially lower than 1.

5.3. Type A3. Finely disseminated gold-pyrite-arsenopyrite ores in tuffaceous sandstones and tuffaceous siltstones

These ores are common in the upper parts of the ore-bearing zone. They are important for the deposit reserves. The ores are mainly hosted in bedded siliceous, siliceous-carbonate tuffaceous sandstones, tuffaceous siltstones, and pyroclastics and consist of scattered pyrite, arsenopyrite and other sulfides. Their contents vary from 3–5 up to 20–30 wt.% with grain sizes rarely exceeding 0.2 mm. According to Sazonov et al. (1998), volcanic and volcano-sedimentary host rocks of the deposit and its immediate surroundings underwent extensive multiple phases of hydrothermal alteration, locally within the fault zones. These changes are represented by propylitization (epidote-chlorite facies) and

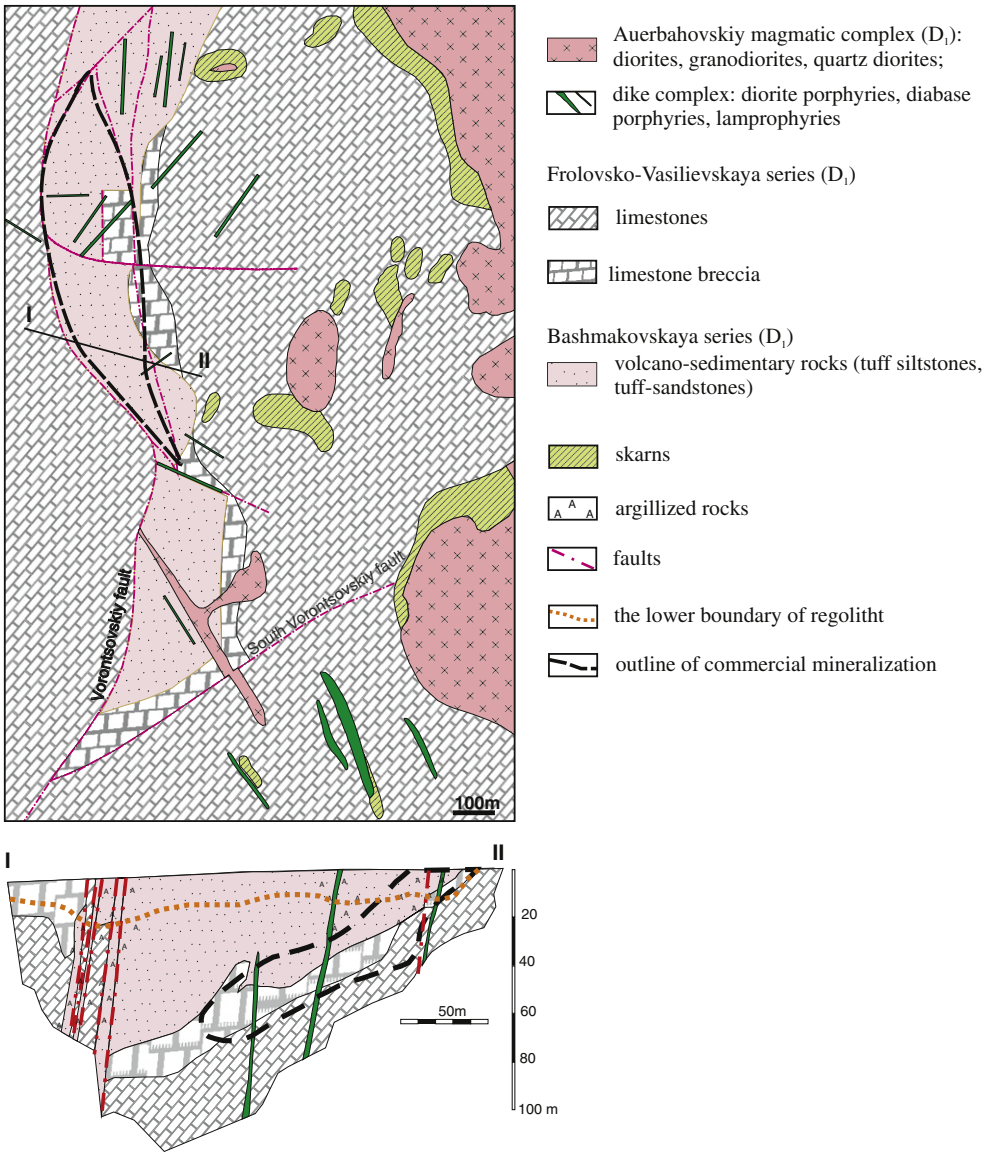

Fig. 3. Geological map of the Vorontsovskoe deposit and cross section profile I–II. Adapted from (Sazonov et al., 1991).

subsequent development of quartz-sericite alteration with progressive increasing in gold content. The gold content in propylitized rocks is as much as 4 ppm.

The outline of commercial gold ores involves volcano-sedimentary rocks commonly altered to quartz-sericite. Here, the gold content may increase by 1–2 orders of magnitude. The ore zones comprise quartz-sericite, quartz-sericite-albite, quartz-sericite-chlorite rocks with scattered pyrite, arsenopyrite, realgar, native arsenic and gold, fahlores, and other sulfides. In places, silicified and sericitized tuffaceous-sandstones and tuffaceous siltstones are cut by a network of carbonate and quartz-carbonate veins (Fig. 4, A). These veins contain rare sulfides and native gold particles with size up to 1 mm. In other cases, the rock is fractured and filled with large aggregates of native arsenic (Fig. 4, C) and realgar (Fig. 4, D).

5.4. Type B1. Finely disseminated gold-pyrite-realgar ores in carbonate breccias

Sulfidized brecciated limestones are the most productive gold-bearing formation. They occur in the central part of the deposit at its deepest horizons. Breccia clasts consist of limestone recrystallized and marmorized to varying degrees. In places, fragments contain scattered realgar, or, rarely, orpiment, giving the rock a reddish-orange or yellow-orange color. Cement of the breccias is composed of altered carbonate-tuffaceous material (Fig. 5). It is saturated by very fine (less than 0.1 mm in size) disseminated pyrite, arsenopyrite, pyrrhotite, and other Zn-Pb-Cu-Hg-Tl-Sb-As sulfides, and contains the major part of native gold particles. Volcanogenic breccia material has undergone changes due to propylitic and quartz-sericite alteration; carbonate constituent of breccia cement, as well as rock fragments, are recrystallized with the formation of coarse-grained calcite aggregates. The Au/Ag ratio in ores is higher than 1.

5.5. Type C1. Gold-oxide-clay ores

The gold-oxide-clay ores (type C1) include ores in regoliths and in karst fillings (Sazonov et al., 1991; Rindzyunskaya et al., 1995). The orebodies occur subhorizontally to a depth of 65 m, whereas in karst cavities they occur at a depth of up to 100 m.

Ores in the regolith are located immediately above the body of primary ores with no change in morphology and bedding. No significant redistribution of gold concentration is observed, and in general it has a

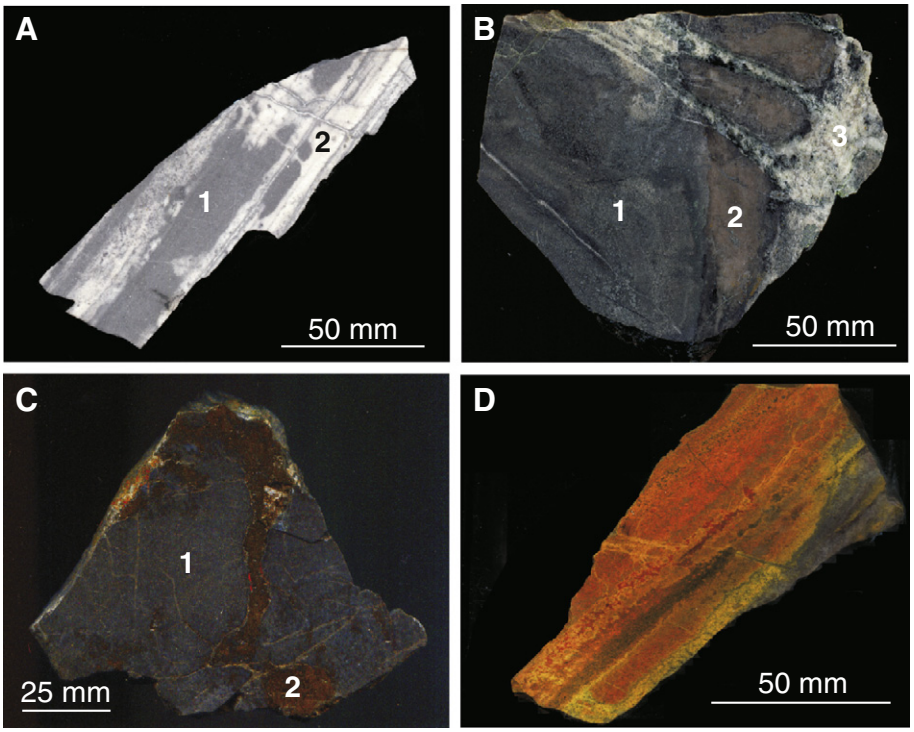

Fig. 4. Type A3 ores: A. tuffaceous siltstone with disseminations of fine pyrite, arsenopyrite, and native gold (1) cut by dark siliceous material with rare enlarged grains of pyrite and native gold (2). Along the silicification zones, one can observe thin carbonate veins; B. tuffaceous siltstone with scattered thin pyrite and native gold (1) and a fragment of limestone (2) cut by veins of quartz-carbonate with rare sulfides and invisible native gold particles (3); C. gold-rich (up to 1000 ppm) tuffaceous siltstone with disseminated pyrite, arsenopyrite, and native arsenic (1) cut by veins of native arsenic and realgar (2). Sample 1589. Northern open pit, hor. + 124 m; D. realgar mineralization in a layered tuffaceous siltstone.

residual character. On the other hand, ores of karst cavities have irregular gold distribution. Here, one can observe both the sites of their dissolution and enrichment with respect to primary ores. In general, gold contents increase from oxidation zone to intense development of iron and manganese hydroxides (Rindzyunskaya et al., 1995).

5.6. Type C2. Gold-sulfide-clay ores

Type C2 ores are products of overprinting of low-temperature argillic alteration processes on the Mesozoic regoliths and karst formations. They are distinctly manifested at the bottom of the regoliths, where clays can be 20–25 m thick (saprolite). The main distinctive feature of the clay formations (argillic alteration) is the presence of unoxidized pyrite and other sulfides, as well as native metals (Pb, Cu, Sn, etc.), and the newly formed native gold. The gold content in the type C2 ores is a few ppm, whereas in pyrite it can be higher than 10 ppm.

Table 1
Characteristics of different ore types at the Vorontsovskoe deposit.

Commercial ore type	Mineral ore type	Type of syn-ore hydrothermal alteration
A. Silicate	A1. Impregnated gold-magnetite-sulfide	Skarn formation, propylitization
	A2. Impregnated gold-polymetallic	Silicification, dolomitization (jasperoids)
	A3. Finely disseminated gold-pyrite-arsenopyrite	Propylitization, silicification, sericitization
B. Carbonate	B1. Finely disseminated pyrite-realgar	Silicification, sericitization
C. Regolith	C1. Gold-oxide-clay	Hypergene oxidation, leaching, hydration, hydrolysis
	C2. Gold-sulfide-clay	Argillization

6. Mineral composition of ores

6.1. Type A1. Disseminated gold-magnetite-sulfide ores in calcareous skarns

Mineralogy of the auriferous skarns at the Vorontsovskoe deposit within the ore zone and skarns located eastward is similar to the skarn-magnetite deposits of the Turinsk-Auerbah ore field (Murzin and Sazonov, 1996, 1999). The early skarn ore assemblage is characterized by low gold content and is composed of two generations of

Fig. 5. Calcified breccia with disseminated realgar (type B1 ore).

Table 2
Composition of gold of Vorontsovskoe deposit; wt.%.

Sample	Au	Ag	Cu	Hg	Total	Fineness, ‰
Ore type A1. Pyrite-pyrrhotite-polymetallic assemblage, generation 1						
396	91.58	6.69	0.05	0.0	98.32	931
	91.00	7.75	0.06	0.0	98.81	921
	90.33	7.86	0.07	0.0	98.26	919
	90.77	7.85	0.04	0.0	98.66	920
Generation 2						
396	60.94	37.40	0.0	0.0	98.34	620
	69.44	28.52	0.0	0.0	97.96	709
	60.02	37.79	0.0	0.0	97.81	614
334	68.16	30.12	0.0	0.72	99.00	688
	68.10	29.74	0.06	1.08	98.98	689
Ore type A2. Impregnated gold-polymetallic. Sulfosalt-polymetallic assemblage, generation 1						
347	92.20	5.50	0.0	0.0	97.70	943
	95.40	5.40	0.0	0.0	100.80	946
	95.30	5.20	0.0	0.0	100.50	948
Sulfosalt-polymetallic assemblage, generation 2						
347	73.30	24.00	0.00	1.00	98.30	746
	79.60	17.70	0.10	0.0	97.40	817
	83.30	15.50	0.10	0.0	98.90	842
	85.40	14.60	0.00	0.0	100.00	854
	84.20	16.10	0.00	0.60	100.90	834
21	75.90	24.30	0.20	0.10	100.50	755
	73.60	26.10	0.10	0.40	100.20	735
	74.00	25.80	0.30	0.30	100.40	737
Polymetallic assemblage						
332	66.50	31.10	0.0	0.0	97.60	681
Ore type A3. As-arsenopyrite assemblage						
1589	93.16	4.97	0.12	1.21	99.46	937
	93.83	5.27	0.20	0.19	99.49	943
	95.35	4.40	0.00	0.00	99.75	956
	93.54	4.72	0.02	1.37	99.65	939
	92.99	5.10	0.09	2.59	100.77	923
	93.28	5.13	0.00	0.12	98.53	947
	93.87	4.86	0.30	0.37	99.40	944
	93.17	5.78	0.19	0.00	99.14	940
	93.26	4.79	0.00	0.39	98.44	947
	94.25	4.24	0.00	0.00	98.49	957
Ore type B1. Pyrrhotite-pyrite assemblage						
276	99.90	0.30	–	–	100.20	998
	97.10	0.80	0.20	0.0	98.10	990
	97.10	0.40	0.20	0.0	97.70	994
	98.10	1.20	0.10	0.0	99.40	987
Orpiment-realgar mineral assemblage						
922	94.35	3.15	0.36	3.29	101.15	933
	94.24	2.13	0.00	0.71	97.08	971
	93.16	2.59	0.04	3.18	98.97	941
	94.07	2.93	0.00	1.15	98.15	958
	91.76	2.69	0.00	3.46	97.91	937
	96.97	1.03	0.00	0.48	98.48	985
	92.74	2.69	0.00	2.06	97.49	951
	94.28	2.87	0.00	1.33	98.48	957
921	97.81	0.14	0.00	1.03	98.98	988
	96.55	0.00	0.00	1.09	97.64	989
	97.55	0.00	0.10	2.97	100.62	969
	97.76	0.13	0.07	2.66	100.62	972
	97.84	0.00	0.44	2.02	100.30	975
701	96.38	0.63	0.00	2.95	99.96	964
	98.52	0.96	0.00	2.20	101.68	969
	97.26	0.31	0.15	1.82	99.54	977
	97.80	0.28	0.00	1.36	99.44	984
	99.12	0.99	0.19	1.43	101.73	974
Ore type C2. Gold-sulfide-clay						
Vor-1	98.50	1.11	0.41	0.09	100.11	984
Vor-33	91.57	2.79	0.49	5.54	100.39	912
	94.03	4.28	0.24	0.00	98.55	954
	98.42	1.41	0.55	0.00	100.38	980
	82.95	14.43	0.45	2.89	100.72	824
	79.43	18.97	0.72	0.00	99.12	801
Vor-63	79.69	19.95	0.22	0.70	100.56	792

(continued on next page)

Table 2 (*continued*)

Sample	Au	Ag	Cu	Hg	Total	Fineness, ‰
	79.20	19.69	0.07	0.77	99.73	794
	79.08	20.74	0.00	0.46	100.28	789
	98.48	0.26	0.48	0.00	99.22	993
	77.33	21.71	0.04	1.46	100.54	769

Sample description: Vor-1 - mica-quartz argillite; Vor-33 - clayey weathering crust; Vor-63 - clay karst formations; 396 - calcite-amphibole-epidote-garnet skarn with pyrite, chalcopyrite and pyrrhotite; 334 - calcite-garnet skarn with pyrite and chalcopyrite; 347 - dolomitic limestone breccia with fine sulfides in cement; 21 - dolomitic limestone with veinlets of sulfides and sulfosalts; 332 - silicified limestone breccia (jasperoids); 1589 - silicified and sericitized tuff siltstones with large segregations of native arsenic; 276 - limestone breccia with sulfides in cement; 921 and 922 - limestone breccia with realgar; 701- silicified limestone breccia with barite-talc-carbonate cement.

magnetite and pyrite. Magnetite of the first generation forms crystal aggregates or xenomorphic grains up to several centimeters in size. The first generation of pyrite is represented by xenomorphic grains up to several mm in size, which are filling the intergranular spaces in magnetite aggregates. The pyrite and magnetite individual grains of the second generation form scattered disseminations in skarns.

Deposition of minerals of late pyrite-pyrrhotite-polymetallic mineral assemblage was preceded by a period of fracturing of early skarns, followed by replacement of skarn minerals (garnet, pyroxene, epidote) by quartz, calcite, and chlorite. The gold content in this mineral assemblage increases and particles of native gold are observed in ores. Ore minerals are represented by pyrite, pyrrhotite, chalcopyrite, sphalerite, galena, and native gold of two generations.

The earliest mineral of the pyrite-pyrrhotite-polymetallic assemblage is pyrite observed in the form of crystals or xenomorphic grains with a size of 1–10 mm in quartz and calcite. Pyrite includes angular or rounded particles of native gold of the first generation. Fineness of gold particles of this generation (Table 2) is high (919–931‰), whereas their size does not exceed 0.05 mm.

Pyrrhotite, chalcopyrite, and minor sphalerite, galena and native gold of the second generation are deposited later than pyrite. These sulfides fill microfractures in pyrite. The size of pyrrhotite and chalcopyrite in quartz and calcite is up to several centimeters. Sphalerite contains finely disseminated chalcopyrite, mainly in the central part of the grains. The impurities in sphalerite are dominated by iron (3.0–10.7 wt.%), with other impurities such as Cu, Hg, Mn, and Cd not exceeding 0.3 wt.%. Native gold particles of the second generation are less than 0.1 mm in size and have a different morphology. For instance, it has streaky and angular forms in pyrite, whereas quartz and calcite are isometric. Fineness of the native gold particles of the second generation is 614–709‰ (Table 2). The impurity components are Ag (28–38 wt.%) and Hg (0.7–1.1 wt.%).

6.2. Type A2. Disseminated gold-polymetallic ores in jasperoids

The sulfosalt-polymetallic mineralization type is associated with the dolomite-ankerite facies of jasperoids, whereas the polymetallic type is associated with quartz. The groundmass of both ore types is composed of quartz and carbonate (dolomite, calcite), with sulfides disseminations of varying intensities in calcareous breccias and tuffaceous siltstones. The chemical composition of typical mineral grains of type B2 ores is shown in Table 3.

6.2.1. Sulfosalt-polymetallic mineralization

Two mineral assemblages are distinguished in this mineralization: early pyrrhotite-arsenopyrite-pyrite and late sulfosalt-polymetallic. The early assemblage is represented by pyrite and arsenopyrite with a size less than 1 mm scattered in quartz-carbonate rock. In places, pyrite crystals form fragmented clusters up to 1–2 cm in size, the fractures of which are filled with minerals of late sulfosalt-polymetallic assemblage. Pyrrhotite crystals less than 0.1 mm in size are included in carbonate.

Formation of the late sulfosalt-polymetallic assemblage started with the deposition of native gold and sulfides of the first generation, i.e. chalcopyrite, sphalerite, and galena, and terminated by deposition of the same minerals of second generation as well as alabandine, Cu-Pb-Sb sulfosalts, and fahlore.

Chalcopyrite of the first generation contains star-like sphalerite inclusions. This sphalerite has emulsion disseminations of chalcopyrite and pyrrhotite, whereas its second generation is free of such inclusions. Sphalerite of the second generation contains 6.4–8.5 wt.% Fe, 0.1–4.9 wt.% Mn, and 0.4–1.3 wt.% Cd (Table 3). The content of Ag and Hg admixtures therein does not exceed 0.3 wt.%, and that of Cu 0.7 wt.%.

Native gold of the first generation has high fineness (943–948, Table 2) with grain size of less than 0.05 mm. It is enclosed in quartz and carbonate, rarely in pyrite. Native gold particles of the second generation are less than 0.04 mm in size and reside in fahlore and in Cu-Pb-Sb sulfosalts (Fig. 6A). Gold fineness of the second generation is essentially lower than that of the first generation and is in the range 735–854 and in contrast to the first generation gold. It has traces of Cu (0.3 wt.%) and Hg (up to 1.0 wt.%).

Alabandite (MnS) is a rare sulfide in the sulfosalt-polymetallic assemblage. Its crystals or individual grains, occasionally overprinting or co-existing with pyrite, are of irregular form and hosted by carbonate. The main impurity component in alabandite is Fe (2.8–3.5 wt.%). The content of other impurities (Zn, Mn, Cd, and Hg) is not higher than 0.1 wt.%.

Cu-Pb-Sb sulfosalts, boulangerite ($Pb_5Sb_4S_{11}$), bournonite ($CuPbSbS_3$) and jamesonite ($Pb_4FeSb_6S_{14}$) are scattered in the limestone as particles of angular shapes or needle-like crystals smaller than 1 mm. In addition, these minerals are filling the cracks in limestone and also occur as veinlets of up to 5 mm thick.

Fahlore concludes the mineral deposition in the sulfosalt-polymetallic assemblage. Fahlore (also referred to as grey ore) is present in the form of disseminations of isometric crystals or grains of irregular form smaller than 0.2 mm in quartz-carbonate or forms rims on the individual grains of chalcopyrite, sphalerite, boulangerite, and bournonite. A specific feature of the chemical composition of fahlore is high content of silver up to 22.5 wt.% (Table 3). Fahlore contains 0–5.3 wt.% Fe and 1.7–7.2 wt.% Zn. Varieties of argentotetrahedrite (6.2–22.5 wt.% Ag), tetrahedrite (0.4–4.6 wt.% Ag) and rare Zn-tetrahedrite-tennantite and Zn-tennantite contain less than 0.2 wt.% Ag. Despite a wide isomorphism of monovalent (Ag, Cu) and divalent (Fe, Zn) metals in fahlore from different samples, variations in the composition within the individual grains are insignificant.

6.2.2. Polymetallic mineralization type

The early sphalerite-pyrite and late mineral assemblages are part of the polymetallic mineralization. Minerals of the early assemblage are composed mainly of pyrite and sphalerite, and minor arsenopyrite and pyrrhotite. The sphalerite and pyrite grains have microfractures filled with quartz, dolomite, or late sulfides.

Sphalerite of the sphalerite-pyrite assemblage contains fine blebs of chalcopyrite (commonly known as chalcopyrite disease; see Craig and Vaughan, 1981). The arsenopyrite and pyrrhotite crystals with the size

Table 3
Composition of sulfide minerals of impregnated gold-polymetallic ores (A2 type, wt.%).

Mineral	Cu	Ag	Fe	Zn	Hg	Mn	Cd	Pb	Sb	As	S	Total
Sulfosalt-polymetallic assemblage,												
Arsenopyrite	0.2	–	34.4	–	–	–	–	–	–	44.1	21.4	100.1
	–	–	34.2	–	–	–	–	–	–	43.9	22.5	100.6
	–	–	34.3	–	–	–	–	–	–	43.7	23.0	101.0
Pyrrhotite[a]	0.0	–	60.3	–	–	–	–	–	–	–	39.3	99.9
	0.0	–	60.3	–	–	–	–	–	–	–	39.2	99.7
Sphalerite	0.0	–	7.13	56.36	0.10	3.55	0.48	–	–	–	33.10	100.72
	0.0	–	6.39	56.25	0.17	4.86	0.44	–	–	–	33.38	101.49
	0.0	–	8.52	56.95	0.13	0.85	1.28	–	–	–	33.59	101.32
Alabandine	0.0	–	3.36	0.0	0.07	60.19	0.10	–	–	–	36.94	100.66
	0.0	–	2.79	0.0	0.0	60.95	0.08	–	–	–	37.02	100.84
Berthonite	13.0	–	0.1	–	–	–	–	43.1	24.5	–	19.6	100.3
	13.5	–	0.2	–	–	–	–	42.8	23.5	–	20.0	100.0
Boulangerite	0.6	–	0.2	–	–	–	–	55.1	25.9	–	19.0	100.8
	0.5	–	0.2	–	–	–	–	55.1	25.8	–	18.9	100.5
Plagionite	0.4	–	0.1	–	–	–	–	41.3	36.1	–	21.1	99.0
	–	–	–	–	–	–	–	41.3	36.4	–	20.9	98.6
Tennantite	40.7	0.2	1.0	6.6	0.7	–	0.0	–	5.1	16.0	28.0	98.3
Tennantite-tetrahedrite	39.0	0.1	2.3	5.7	0.4	–	0.1	–	16.4	7.7	25.6	97.3
	39.5	0.0	1.3	7.0	0.1	–	0.3	–	19.3	6.3	25.8	99.6
Tetrahedrite	28.7	13.7	0.1	6.3	0.0	–	0.1	–	26.4	1.9	21.6	98.8
	22.4	22.5	1.8	5.8	0.0	–	0.3	–	25.7	1.1	20.6	100.2
	37.8	0.4	0.5	6.8	0.9	–	0.0	–	23.9	4.9	24.8	100.0
	32.8	4.6	5.3	1.8	0.0	–	0.1	–	27.8	0.5	24.5	97.4
Polymetallic assemblage												
Arsenopyrite	–	–	34.8	–	–	–	–	–	–	43.1	22.1	100.0
	–	–	34.2	–	–	–	–	–	–	43.5	21.4	99.1
	–	–	34.1	–	–	–	–	–	–	42.5	21.5	98.1
Pyrrhotite	–	–	60.7	–	–	–	–	–	–	0.0	39.7	100.4
Sphalerite	0.0	–	0.74	66.10	0.09	0.13	0.19	–	–	–	32.47	99.72
	0.0	–	0.57	66.19	0.12	0.0	0.57	–	–	–	32.73	100.18
	0.11	–	0.26	65.26	0.0	0.24	0.62	–	–	–	33.61	100.10
Tennantite	42.4	0.3	3.1	5.3	0.1	–	0.1	–	0.1	19.9	28.4	99.7
	40.6	0.7	3.6	4.2	0.0	–	0.0	–	5.0	15.5	28.4	98.0
Tennantite-tetrahedrite	39.4	0.7	1.1	7.2	0.2	–	0.0	–	19.0	6.9	25.6	100.1
	39.7	0.5	7.7	0.4	0.0	–	0.0	–	11.1	11.9	27.2	98.5
Tetrahedrite	36.1	2.3	1.3	6.4	0.2	–	0.3	–	28.8	0.0	25.0	100.4
	20.2	22.4	5.7	1.0	0.1	–	0.3	–	28.6	0.0	22.6	100.9
	25.7	15.9	3.3	4.1	0.2	–	0.0	–	25.7	1.4	23.7	100.0

[a] Pyrrhotite contains 0.1–0.2 wt.% of Ni and Co.

less than 0.1 mm form dispersed impregnations in quartz-carbonate mass.

The late polymetallic mineral paragenetic sequence, based on textural relationships, is as follows: sphalerite ➔ chalcopyrite ➔ lead sulfosalts ➔ fahlore ➔ galena ➔ native gold.

The central parts of the sphalerite grains in the polymetallic mineral assemblage contain blebs of chalcopyrite (chalcopyrite disease, mentioned above) and pyrrhotite; whereas such inclusions are absent in the rims. The iron content (0.1–0.7 wt.%) in inclusion-free parts of sphalerite grains is significantly lower relative to sphalerite of the sulfosalt-polymetallic assemblage (Table 3).

The Pb-sulfosalts contain plagionite ($Pb_5Sb_8S_{17}$) and geocronite ($Pb_5(As, Sb)_2S_8$). These minerals in the form of prismatic crystals or xenomorphic grains are less than 0.1 mm in size and included in quartz and carbonate. Rarely, they form intergrowths with galena and arsenopyrite.

Fahlore in the polymetallic mineral assemblage contains zinc (0.4–8.0 wt.%) and iron (0.5–7.7 wt.%), tennantite-tetrahedrite, and tetrahedrite (Table 3). Grains of tennantite-tetrahedrite are concentrically zoned. Their central parts are Sb-rich, whereas the margins are As-rich. The Ag content increases from tennantite to tetrahedrite from 0.1 to 22.4 wt.%. The most abundant Ag-enriched fahlore can be attributed to freibergite.

Native gold particles smaller than 0.05 mm form the intergrowths with galena or included into it (Fig. 6B). Fineness is less than 700‰, which corresponds to electrum (Table 2).

6.3. Type A3. Finely disseminated gold-pyrite-arsenopyrite ores in tuffaceous-sandstones and tuffaceous siltstones

The ores are represented by propylitic and quartz-sericite hydrothermal alteration. Propylitized rocks are composed of fine-grained aggregates of relic pyroxene, plagioclase, carbonate and the newly-formed minerals, including actinolite, epidote, chlorite, quartz, albite, K-feldspar, sericite, calcite, hydromica, and zeolites (Sazonov et al., 1991; Rovnushkin et al., 2010). In some cases, adularia may be present, a diagnostic mineral of low-sulfidation epithermal systems. Adularia (triclinic coefficient 0.59) replaces albite in the propylitic altered volcanics. Mineral balance calculations of Au from the sample of quartz-adularia-chlorite-carbonate altered rocks showed that whereas Au content in K-feldspar is about 6.3 ppb, adularia contains few tens of ppm Au, and adularia with sulfides contains few tens ppm (Sazonov et al., 1991).

Ore minerals in the propylitic rocks consist of disseminated pyrite and arsenopyrite. The grain size of these sulfides ranges from less than 0.05 mm to 2–3 mm. Pyrite contains 0.09–0.36 wt.% As (Table 4). Arsenopyrite has low-As (40.7–42.2 wt.% As) contents. Native gold in this ore type is represented by irregular disseminations of its particles scattered mainly in the body of rock, rarely in the intergrowths with sulfides. In the areas of quartz-sericite alteration, the amount of gold particles increases significantly.

The Au-richest (higher than 1000 ppm Au) sites of brecciated tuffaceous siltstones are associated with intense silicification and sericitization ($2M_1$ sericite modification). Here, a scattered

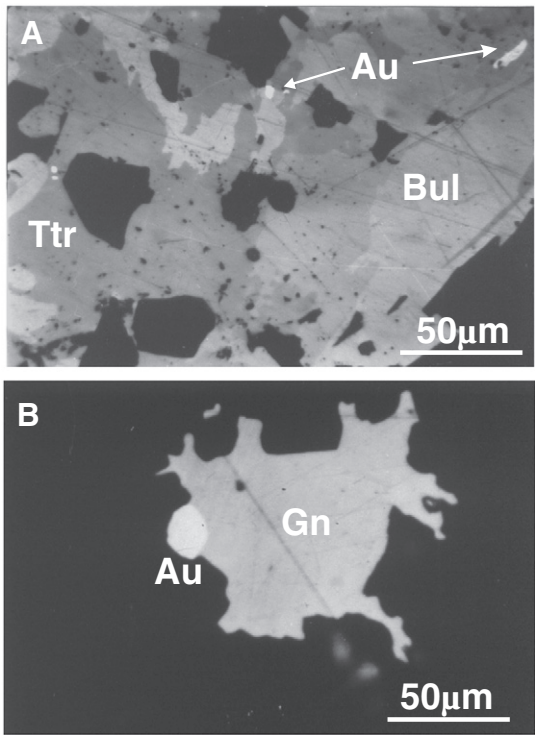

Fig. 6. Particles of native gold in type A2 ores. A. Sulfosalt-polymetallic mineral assemblage. Fine particles of native gold (Au) in boulangerite (Bul) and tetrahedrite (Ttr) aggregate. B. Polymetallic mineral assemblage. Crystal of native gold (Au) intergrown with galena (Gn) in quartz. Photomicrographs in reflected light.

impregnation of ore minerals of the arsenic-arsenopyrite assemblage, arsenopyrite, native Au, and As with the grain size of 0.5 mm and smaller is developed (Fig. 7A). Disseminated ore is intersected by brecciated zones of 5 cm thick, to which the veinlets of native gold segregations (up to 2–3 cm thick) are confined (Fig. 4C). The ore process is terminated by the formation of thin quartz-realgar veinlets up to 5 mm thick that intersect the ore zones.

The sericite-quartz altered rocks contain a small amount of apatite, rutile, titantite, and calcite with a size typically less than 0.02 mm, rarely 0.1 mm. Apatite belongs to the variety containing fluorine (2.5–2.7 wt.%) and chlorine (0.8–1.2 wt.%). Calcite inclusions in the native arsenic (Fig. 7B) are characterized by a high content of Mg (0.66 wt.%) and Mn (2.21 wt.%).

Arsenopyrite is represented by two morphological varieties which are present in the altered rocks approximately in equal amounts (Fig. 7C). The first arsenopyrite variety is represented by crystals with size less than 20 μm, cemented by quartz or native arsenic. Another arsenopyrite variety is represented by prismatic crystals up to 0.5 mm in size. Both varieties contain high-arsenic (47.0–48.2 wt.% As; S/As = 0.93–0.74) (Table 4). Native arsenic is almost pure, as it contains no impurities, the content of which would be higher than the analytical uncertainty. Its surface is rapidly oxidized and covered with a black film of arsenolite (As_2O_3).

Native gold particles are confined to the fine-grained arsenopyrite and enclosed in native As, especially in marginal parts of the large grains of native As (Fig. 7D). Less commonly, they are confined in sericite-quartz, forming close intergrowths with arsenopyrite of both morphological varieties and native As (Fig. 7E, F). The most common are gold particles with a size less than 20 μm. Minor particles are of 50 μm, and only individual grains are large (up to 0.2 mm). The Au is of high fineness (923–956). Individual gold particles contain high levels of Hg (see. Table 2) The highest Hg content (up to 2.6 wt.%) in enclosed in the native As.

In addition to the common sulfides of the arsenic-arsenopyrite mineral assemblage, we found rare amounts of minerals such as sphalerite, alabandite, and fahlore. Rounded grains of these sulfides up to 50–70 μm in size are enclosed in native As or arsenopyrite. A specific feature of sulfide minerals is some Mn impurity in their composition. Mn is present in sphalerite (7.6 wt.%) and fahlore (up to 3.3 wt.%) (Table 4).

6.4. Type B1. Finely disseminated gold-pyrite-realgar ores in carbonate breccias

Rock-forming minerals in the cement of breccias are almost the same as those that host the ores in volcano-sedimentary rocks. Relic minerals of volcanic rocks are pyroxene and plagioclase. Propylitic

Table 4
Composition of sulfide minerals of finely disseminated gold-pyrite-arsenopyrite ores (A3 type, wt.%).

Mineral	Cu	Ag	Fe	Zn	Mn	Cd	Ni	Co	Sb	As	S	Total
Pyrite-arsenopyrite assemblage												
	–	–	45.87	–	–	–	0.02	–	–	0.31	52.64	98.84
	–		45.81	–	–	–	0.02	–	–	0.16	53.27	99.26
	–	–	45.33	–	–	–	0.07	–	–	0.36	52.58	98.34
	–	–	45.59	–	–	–	0.04	–	–	0.09	53.01	98.73
Pyrite	–	–	45.83	–	–	–	0.02	–	–	0.18	53.04	99.43
	–	–	34.62	–	–	–	0.02	–	–	42.15	21.77	98.56
Arsenopyrite	–	–	35.14	–	–	–	0.07	–	–	40.74	22.69	98.64
As-arsenopyrite assemblage												
Arsenopyrite	–	–	33.68	–	–	–	0.02	0.01	–	48.15	18.19	100.05
	–	–	32.66	–	–	–	0.05	0.12	–	48.14	18.17	99.14
	–	–	33.11	–	–	–	0.00	0.00	–	47.30	18.59	99.00
	–	–	33.24	–	–	–	0.13	0.00	–	47.54	18.21	99.12
	–	–	33.54	–	–	–	0.06	0.26	–	47.04	18.67	99.57
Sphalerite	0.0	–	0.69	55.55	7.62	0.09	–	–	–	–	33.57	97.52
Alabandite	0.00	–	0.60	0.11	63.32	0.05	–	–	–	–	36.49	100.57
Tennantite	41.89	0.00	3.15	4.31	0.35	0.00	–	–	3.70	18.48	27.85	99.73
Tennantite-tetrahedrite	40.05	0.00	1.08	7.86	0.00	0.10	–	–	13.29	10.83	26.76	99.97
	38.27	0.10	0.86	3.80	2.60	0.00	–	–	12.73	11.91	27.48	97.75
Tetrahedrite	38.80	0.07	2.62	0.17	3.20	0.00	–	–	25.68	3.25	26.01	99.80
	–	–	0.14	–	–	–	–	–	0.33	99.58	0.08	100.13
	–	–	0.01	–	–	–	–	–	0.12	99.00	0.12	99.25
	–	–	0.00	–	–	–	–	–	0.06	99.31	0.06	99.43
Native arsenic	–	–	0.00	–	–	–	–	–	0.08	99.10	0.00	99.18

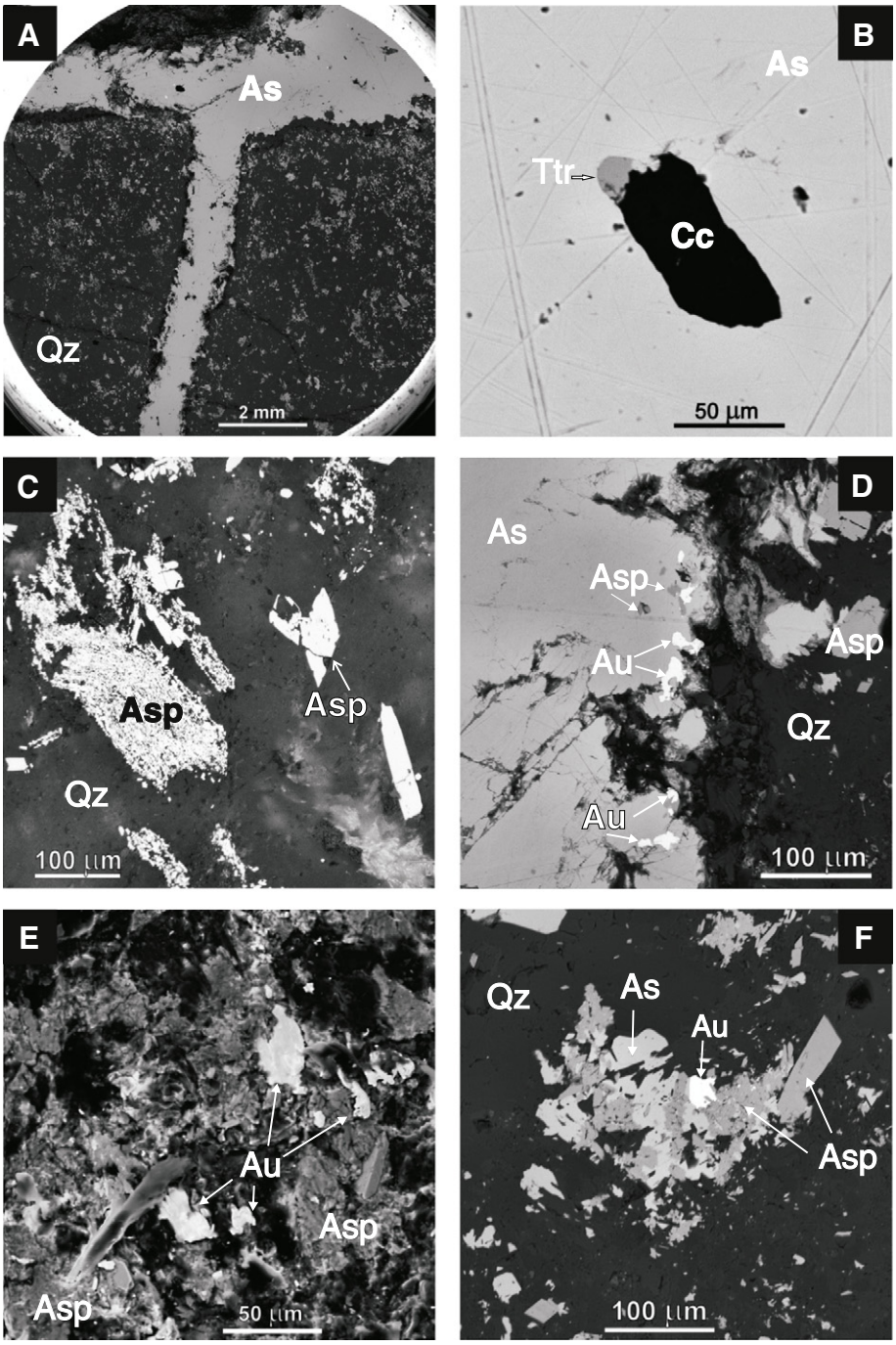

Fig. 7. Minerals of As and arsenopyrite assemblages (type A3 ores): A. tuffaceous siltstones silicified (Qz) with disseminated arsenopyrite and native As, intersected by veins of native arsenic (As); B. intergrowth of tetrahedrite (Ttr) and calcite (Cc) in native As; C. two morphological varieties of arsenopyrite (Asp) in silicified tuffaceous siltstone (Qz); D. concentration of native gold particles (Au) in the edge of a large grain of native arsenic (As) in silicified tuffaceous siltstone (Qz); E. morphology of the surface of a sample of silicified tuffaceous siltstone with particles of native gold (Au) and arsenopyrite prismatic crystals (Asp); F. aggregate of native gold (Au), arsenic (As), and arsenopyrite of two morphological varieties (Asp). Images were obtained on the SEM in the BSE (AD, F) and SE + BSE (E) modes.

alteration minerals are represented by actinolite, chlorite, quartz, K-feldspar, albite, wollastonite, prehnite, and pumpeliite. Quartz-sericite alteration is accompanied by an increase in quartz content, an appearance of $2M_1$ sericite modification, calcite, barite, and apatite.

The chemical composition of relic calcite in limestone is almost pure. The concentrations of oxide impurities (FeO, MgO and MnO) do not exceed 0.3 wt.%. The newly formed calcite of breccia cement is a manganoan calcite which contains 3.6–6.9 wt.% of MnO.

Apatite occurs as fine isometric grains (5–20 μm) in aggregates of rock-forming minerals in breccia cement and manganoan calcite. It is unusual compositionally and corresponds to As fluorapatite (1.8–7.6 wt.% As_2O_3 and 2.4–3.7 wt.% F). The Cl concentration in it does not exceed 0.4 wt.%.

Barite is one of the latest minerals in the breccia cement and occurs in small amounts. Barite grains of 1–2 mm in size cement the space between the rock-forming minerals and pyrite. It contains up to 1.5 wt.% of SrO.

Ore mineral species in carbonate breccias rarely exceed 5 vol.%. However, the bulk of the ore minerals is represented by only two minerals, the ubiquitous pyrite and locally developed realgar. Pyrite crystals with a size less than 0.1 mm also occur in the breccia cement. Realgar is dispersed both in cement and in carbonate fragments in the breccias.

Table 5
Composition of sulfide minerals of the finely disseminated pyrite-realgar ores (B1 type. wt.%).

Mineral	Cu	Fe	Zn	Hg	Tl	Mn	Cd	Pb	Ni	Co	Sb	As	S	Total
Pyrrhotite-arsenopyrite mineral assemblage														
Pyrite	0.17	46.81	–	–	–	–	–	–	0.01	0.31	–	0.16	53.12	100.58
	0.15	46.36	–	–	–	–	–	–	0.10	0.28	–	0.34	53.25	100.48
	0.24	46.57	–	–	–	–	–	–	0.10	0.00	–	0.21	52.39	99.51
	0.0	45.85	–	–	–	–	–	–	0.01	0.46	–	0.40	51.34	98.06
	0.31	46.05	–	–	–	–	–	–	0.37	0.42	–	0.05	51.49	98.69
Arsenopyrite	0.0	35.88	–	–	–	–	–	–	0.14	0.03	–	42.97	21.95	100.97
	0.0	37.16	–	–	–	–	–	–	0.18	0.22	–	39.49	23.87	100.92
	0.07	35.51	–	–	–	–	–	–	0.24	0.18	–	43.61	20.70	100.31
Arsenopyrite-gersdorffite	0.0	12.43	–	–	–	–	–	–	22.02	0.12	–	42.19	20.32	97.08
	0.15	15.80	–	–	–	–	–	–	20.33	0.27	–	43.72	19.80	100.07
Sphalerite	–	0.81	65.21	0.16	–	0.0	0.24	–	–	–	–	–	33.31	99.73
	–	1.18	64.94	0.12	–	0.0	0.17	–	–	–	–	–	33.11	99.52
	–	2.03	64.60	0.09	–	0.0	0.41	–	–	–	–	–	32.04	99.17
	–	0.98	65.75	0.0	–	0.0	0.56	–	–	–	–	–	32.86	100.15
Orpiment-realgar mineral assemblage														
Sphalerite	0.05	0.41	58.69	4.91	–	1.74	0.58	–	–	–	–	–	32.54	98.92
	0.0	0.28	60.83	7.15	–	0.88	0.21	–	–	–	–	–	31.02	100.37
	0.0	0.25	60.73	5.96	–	0.50	0.79	–	–	–	–	–	31.12	99.35
	0.0	0.22	55.33	6.23	–	5.53	–	–	–	–	–	–	32.37	99.68
	0.0	0.16	47.70	18.61	–	4.46	0.39	–	–	–	–	–	30.29	101.60
Alabandite	0.0	0.0	–	0.0	–	64.07	–	–	–	–	–	–	36.77	100.84
	0.0	0.04	–	0.0	–	63.52	–	–	–	–	–	–	37.02	100.58
Boulangerite	–	0.0	–	–	–	–	–	53.90	–	–	26.20	–	18.80	98.90
Jamesonite	0.10	3.30	–	–	–	–	–	39.60	–	–	35.20	–	21.40	99.60
	–	2.10	–	–	–	–	–	39.70	–	–	34.40	–	22.40	98.60
Zinkenite	0.60	0.10	–	–	–	–	–	34.00	–	–	40.20	–	22.10	97.00
	0.60	0.10	–	–	–	–	–	34.30	–	–	39.90	–	22.20	97.10
Chalcostibite	25.60	0.10	–	–	–	–	–	0.0	–	–	48.10	–	25.60	99.40
Aktashite	22.70	–	3.85	32.15	–	–	–	–	–	–	1.19	16.36	24.74	100.99
	24.28	–	1.20	32.16	–	–	–	–	–	–	0.81	16.61	24.98	100.04
	24.34	–	1.44	32.65	–	–	–	–	–	–	0.99	16.02	24.74	100.18
Klerite	–	–	–	–	–	12.84	–	–	–	–	54.46	3.00	30.20	100.50
	–	–	–	–		12.19	–	–	–	–	53.66	2.99	30.75	99.59
	–	–	–	–	–	12.40	–	–	–	–	52.02	3.67	30.63	98.72
Mn-As-Sb-S mineral	–	–	–	–	–	15.24	–	–	–	–	36.24	14.17	33.67	99.32
	–	–	–	–	–	15.14	–	–	–	–	36.36	14.27	33.36	99.13
	–	–	–	–	–	15.40	–	–	–	–	32.31	17.36	33.60	98.67
Chabourneite	–	–	–	–	23.98	–	–	5.99	–	–	31.72	15.85	23.99	101.53
	0.17	–	–	–	23.27	–	–	2.82	–	–	35.09	13.93	24.38	99.66
Ruterite	6.43	–	0.37	35.62	20.18	–	–	0.00	–	–	6.04	11.32	19.06	99.02
	6.39	–	0.78	34.28	21.21	–	–	0.00	–	–	5.58	11.69	20.22	100.15
	6.36	–	0.77	36.72	18.93	–	–	0.00	–	–	5.81	11.46	19.22	99.27
Pierrotite	–	–	–	–	21.96	–	–	–	–	–	36.90	14.80	26.60	100.26
	–	–	–	–	24.32	–	–	–	–	–	33.95	15.85	26.03	100.15
	–	–	–	–	23.59	–	–	–	–		34.45	16.17	26.18	100.39
Realgar	–	–	–	–	–	–	–	–	–	–	0.58	69.88	29.62	100.08
	–	–	–	–	–	–	–	–	–	–	0.22	69.52	28.80	98.54
	–	–	–	–	–	–	–	–	–	–	0.20	69.63	29.66	99.49
Orpiment	–	–	–	–	–	–	–	–	–	–	1.98	59.63	39.11	100.72
	–	–	–	–	–	–	–	–	–	––	0.43	60.81	38.87	100.11
	–	–	–	–	–	–	–	–	–	–	0.56	61.11	39.08	100.75
Stibnite	–	–	–	–	–	–	–	–	–	–	70.83	1.86	27.92	100.61
	–	–	–	–	–	–	–	–	–	–	65.84	5.78	27.85	99.47
	–	–	–	–	–	–	–	–	–	–	64.67	7.49	28.71	100.87
	–	–	–	–	–	–	–	–	–	–	69.31	3.56	27.47	100.34

Table 6
Content of organic matter and its soluble species in different rocks.

Rocks	mg/kg		wt.%	
	n	SOM	n	C_{org}
Cement of ore-bearing limestone breccias	5	57–466 149	4	0.09–0.75
Volcanogenic-sedimentary, including altered rocks	8	23–132 68	4	<0.05–0.75
Metasomatic rock at the contact of subvolcanic dike and limestone	3	77–437 201	3	<0.05–0.09
Massive limestone	1	27	1	<0.05

Notes: SOM - soluble species of organic matter (numerator - the minimum and maximum values in the denominator - the average); C_{org} – total content of organic matter.

Pyrite is the earliest sulfide in the carbonate breccias, formed during propylitic alteration of the cementing material. Its low As content (0.05 to 0.4 wt.%) is the same as in the pyrite of the pyrite-arsenopyrite mineral assemblage in propylitized volcano-sedimentary rocks (Table 5).

The deposition of ore minerals in two auriferous mineral assemblages (early pyrrhotite-arsenopyrite and late orpiment-realgar) is related to the quartz-sericite hydrothermal alteration in carbonate breccias.

The early pyrrhotite-arsenopyrite assemblage consists of arsenopyrite, pyrrhotite, chalcopyrite, sphalerite, and native gold. Arsenopyrite is generally present in the form of clusters of short-prismatic crystals less than 0.05 mm in size (Fig. 8A) or, rarely, as individual zoned crystals up to 0.2 mm, scattered in the cement. The central parts of these crystals are more S-rich and As-poor relative to their rims. The inclusions of

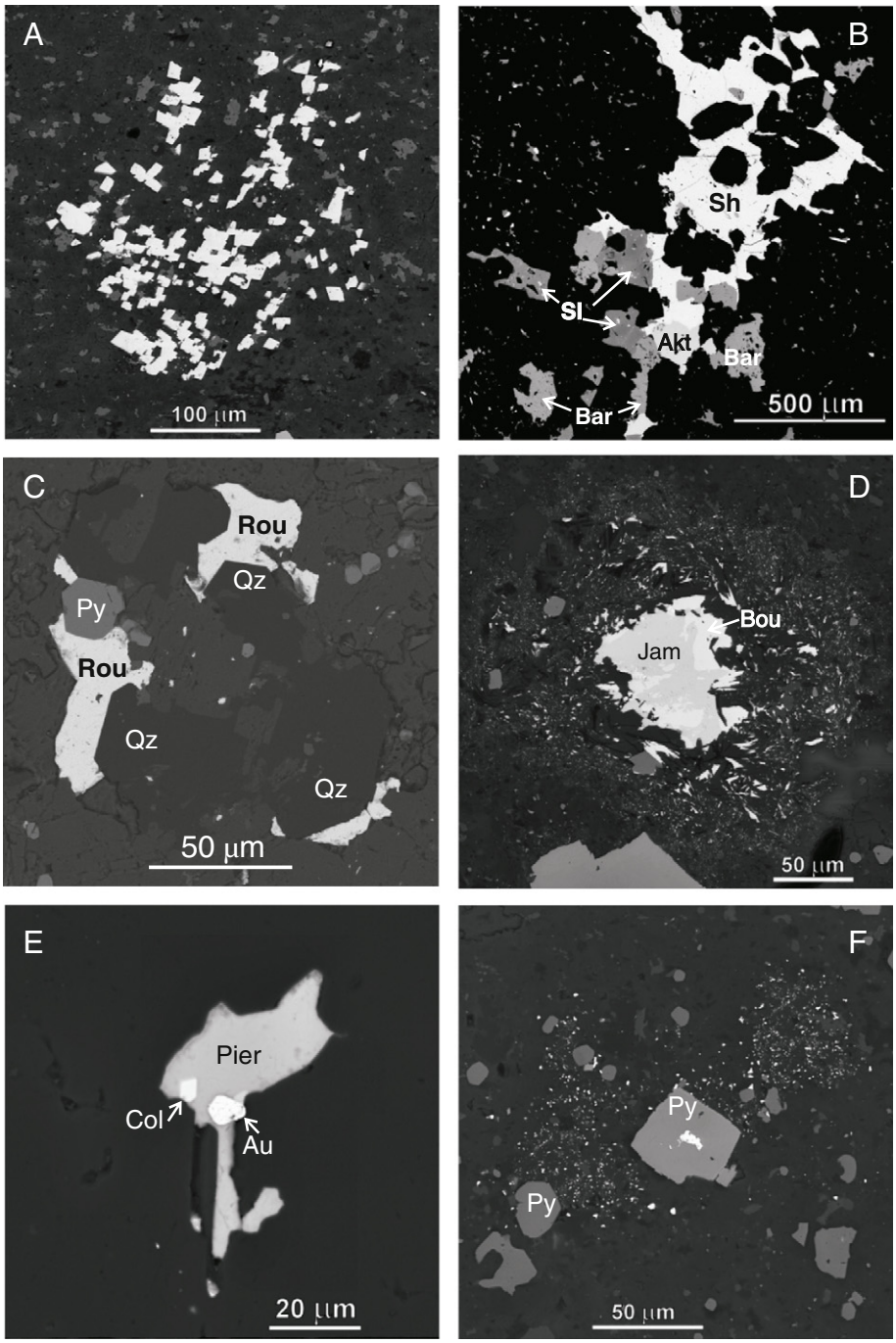

Fig. 8. Ore minerals in the calcareous breccia (type B1): A. scattered thin pyrite (dark grey) and accumulations of arsenopyrite crystals (white) in the cement of calcareous breccia; B. aggregate of chabourneite grains (Sh), aktashite (Act), sphalerite (Sl), and barite (Bar) in nonmetallic minerals; C. xenomorphic segregations of routhierite (Rou) intergrown with crystals of quartz (Qz) and pyrite (Py); D. jamesonite (Jam) intergrown with bournonite (Bou) with a halo of fine particles of Hg and Tl sulfosalts; E. xenomorphic segregations of pierrotite (Pier) with inclusions of the crystals coloradoite (Col) and native gold (Au); F. "cloudy" accumulation of small particles of native gold (white) in limestone breccia cement with disseminated pyrite (Py). Images were obtained on the SEM in the BSE mode.

sulfoarsenide of the arsenopyrite-gersdorffite series are 10–20 μm in size and are also contained in pyrite (Table 5). Pyrrhotite, chalcopyrite, and sphalerite occur as rounded or angular inclusions in pyrite and arsenopyrite and, rarely, as grains up to 0.2 mm, enclosed in host rocks. Sphalerite grains in their central parts contain finely disseminated chalcopyrite. The inclusion-free rims contain impurities of Fe (0.8–2.0 wt.%), Cd (0.2–0.6 wt.%), and Hg (up to 0.16 wt.%) (Table 5). The native gold particles in the pyrrhotite-arsenopyrite assemblage are of rounded or irregular shapes. They are located in non-metallic minerals and have a size of about 0.02 mm. Gold fineness is very high (987–998; Table 2).

The orpiment-realgar mineral assemblage is made up of the following minerals: As-Sb sulfides (realgar, orpiment, and stibnite), Hg (cinnabar), Zn (sphalerite), and Mn (alabandite); Mn sulfur-arsenite-stibnites (klerite) and X phase (Mn-As-Sb-S); Hg sulfosalts (aktashite), Tl (ruterite, pierrotite, chabourneite), Pb and Cu (jamesonite, boulangerite, zinkenite, chalcostibite); Hg telluride (coloradoite); and

native As and Au. All minerals of this assemblage have a complex morphology controlled by filling cavities of various sizes.

Realgar (AsS) is the most common sulfide of the orpiment-realgar mineral assemblage. It forms the scattered angular separations of less than 1 mm in cement and breccia clasts. The larger (up to 3–5 mm) realgar grains fill cavities and fractures that intersect the breccias. Sphalerite, Tl and Hg sulfosalts are observed as inclusions in realgar.

Orpiment (As_2S_3) is rare, forming grains of up to 1 mm in size, occasionally with realgar inclusions.

Stibnite (Sb_2S_3) forms angular grains and rare crystals up to 0.1 mm, occasionally up to a few mm, in carbonate. It also forms the intergrowths with Hg, Tl, Pb and Cu sulfosalts (aktashite, pierrotite, zinkenite, chalcostibite). The chemical composition of As sulfides is characterized by the presence of Sb impurities (up to 2 wt.%), whereas Sb contains up to 7.5 wt.% of As (Table 5).

Alabandite (MnS) occurs as crystals of up to 0.15 mm in breccia cement and also occurs as inclusions in realgar. Alabandite has a stoichiometric composition (Table 5).

Sphalerite (ZnS) forms individual grains varying in size from 0.05 to 0.2 mm in the barren minerals of the breccia cement. It is also found as intergrowths with barite, pyrite, and Hg-Tl sulfosalts (Fig. 8B). A specific compositional feature of sphalerite in the orpiment-realgar assemblage is the high concentration of Mn (up to 5.5 wt.%) and of Hg (up to 18.6 wt.%) (Table 5).

Cinnabar (HgS) is a rare ore mineral. The grains of 0.1–0.3 mm in size are observed in association with realgar in carbonate veinlets intersecting carbonate breccia. No impurities were found in its mineral composition.

The Mn sulfoarsenostibnides are represented by klerite ($MnSb_2S_4$), discovered for the first time at the Vorontsovskoe deposit (Murzin et al., 1996), and a new Mn-As-Sb-S phase. Klerite grains smaller than 0.4 mm form intergrowths with realgar, and Hg-Tl sulfosalts, or embedded in these minerals. Klertite contains about 4.3 wt.% of As (Table 5). The Mn-As-Sb-S phase has high As content (14.2–17.4 wt.%), which is higher than that in klerite.

Aktashite ($Cu_6Hg_3As_4S_{12}$) is represented by segregations of 0.15 mm in size. It is often found in intergrowths with sphalerite and Tl sulfosalts (Fig. 8B). In addition to the main components, it contains impurities of Zn (1.2–3.85 wt.%) and Sb (0.63–2.81 wt.%; Table 5).

Arsenic-antimony sulfosalts of thallium commonly occur in carbonate breccias. Their xenomorphic grains form intergrowths with quartz, calcite, barite, pyrite and ore minerals (Fig. 8B, C) and have a size of less than 0.05 mm, but occasionally up to 0.5 mm. The poor knowledge of this mineral group makes it difficult to assign them to a mineral type only by chemical composition. Nevertheless, we can confidently distinguish three groups of sulfosalt: thallium, lead-thallium, and copper-mercury-thallium (Table 5). The chemical composition of Tl sulfosalt corresponds to the pierrotite formula ($Tl_2Sb_6As_4S_{16}$), which has the similar As/Sb ratio. However, it may also be attributed to parapierrotite Tl $(Sb, As)_5S_8$ or bernardite $Tl(As, Sb)_5S_8$. The Pb-Tl sulfosalt is conventionally attributed to shaburneite $(Tl, Pb)_{21}(Sb, As)_{91}S_{147}$, the closest analogue on the basis of the main component ratios. This sulfosalt, however, is poorer in Pb and S as compared to the shaburneite empirical formula. Cu-Hg-Tl-sulfosalt is identified by chemical composition (Table 5), optical and X-ray properties (Sazonov et al., 1991) and belongs to routhierite (Tl, Cu) (Hg, Zn) $(As, Sb)_2S_3$.

The lead and copper sulfosalts-jamesonite ($Pb_4FeSb_6S_{14}$), boulangerite ($Pb_5Sb_4S_{11}$), zinkenite ($PbSb_2S_4$), and chalkostibite ($CuSbS_2$) form disseminations of particles less than 0.5 mm in the nonmetallic part of the breccia cement. These minerals commonly occur as intergrowths with one another, as well as with stibnite (Fig. 8D). The chemical composition of the minerals is shown in Table 5.

Coloradoite (HgTe) is a rare mineral in the deposit. Grains of this mineral of up to 0.1 mm in size are associated with native arsenic, gold, and pierrotite (Fig. 8E). The chemical composition of the coloradoite grains corresponds to its stoichiometric composition.

Native arsenic is represented by isometric crystals or xenomorphic segregations of up to 1 mm, enclosed in the barren minerals of breccia cement and limestone clasts. It is also found in the form of fine inclusions (0.002–0.015 mm) in stibnite. No impurities in amounts of more than 0.1 wt.% were identified in native arsenic composition.

Native gold of orpiment-realgar mineral assemblage is represented by particles less than 0.1 mm, typically less than 0.02 mm. They form disseminations in the gangue and nonmetallic minerals of the breccia cement such as quartz, carbonate, barite, rarely, in arsenopyrite, sphalerite, pierrotite and other ore minerals (Fig. 8E). In places, gold particles (<0.005 mm) are present in breccia cement as patches with thick "cloud" segregations (Fig.8G). Gold in this mineral assemblage is of a high fineness (930–990) and contains 0.7–3.5 wt.% of Hg (Table 2).

6.5. Type C1. Gold-oxide-clay ores

The regolith was thoroughly studied by Sazonov et al. (1991) and Rindzyunskaya et al. (1995). According to these authors, dissolution, hydration and leaching zones can be distinguished in these mineralized regolith materials.

The hydration of mica and mafic minerals, as well as the partial oxidation of the primary sulfides with the formation of limonite pseudomorphs, occur within the zone of dissolution. The silt-clay fraction preserves minerals of primary rocks, and it also contains newly formed minerals, such as gypsum, halloysite, minor kaolinite and jarosite. The hydration and leaching zone is composed of partially weathered rock fragments and clay material (lower saprolite; Taylor and Eggleton, 2001), up to the clay at the top of the section (upper saprolite; Taylor and Eggleton, 2001; Freyssinet et al., 2005; Anand, 2011). The clay fraction is composed of kaolinite, smectite, hydromicas, and chlorite, with minor amounts of halloysite and jarosite. The heavy fraction is dominated by Fe and Mn hydroxides and includes rare relicts of pyrite.

The leaching and hydrolysis zone is represented by amorphous clays. The rock-forming minerals and sulfides are almost completely leached out. Clay minerals are mainly kaolinite, occasionally halloysite and 1M-polytype mica.

Native gold in the regoliths is mainly residual. Its particles carry traces of supergene alteration (development of high-grade shell corrosion), increasing towards the top of the weathering profile (Fig. 9).

The karst deposits are mainly composed of kaolinite. Residual minerals are barely preserved. In places, strong ferrugination is manifested, up to the formation of brown hematite lenses. Residual particles of native gold have a high degree of supergene alteration (deep corrosion, roundness, traces of mechanical deformation). Karsts contain also secondary native gold; its amount increases in sediments of the redeposited regoliths.

6.6. Type C2. Gold-clay-sulfide ores from argillic zones

The karst regoliths are composed of multicolored clay materials (kaolinite, montmorillonite, illite, and smectite), quartz, carbonates (calcite, dolomite, siderite), goethite, and pyrite (1 wt.%).

Minerals formed during argillisation are hydromica (illite), carbonates (dolomite, calcite, siderite), barite, quartz and ore minerals. Ore minerals are represented by pyrite, accompanied by arsenopyrite, native gold and rare galena, sphalerite, chalcopyrite, stibnite and fahlore.

Pyrite from the argillic zones is present in varying amounts from single grains up to 1–5 wt.%, and occasionally more. It is represented by crystals of cubic habitus or combining cube and pentagondodecahedral faces. The crystals are small in size (more than 90% of the grains are less than 0.5 mm). A specific feature of pyrite from argillized rocks is the presence on its crystal surfaces of newly formed mineral phases (Azovskova et al., 2013a,b). Among these phases, found in 42% of the 300 studied pyrite crystals, we recognized native metals (gold, copper and zinc copper, lead), sulfides (galena, arsenopyrite, stibnite, chalcopyrite, copper sulfides, sphalerite, Ni-Co-Cu sulfoarsenides), sulfosalts (Zn,

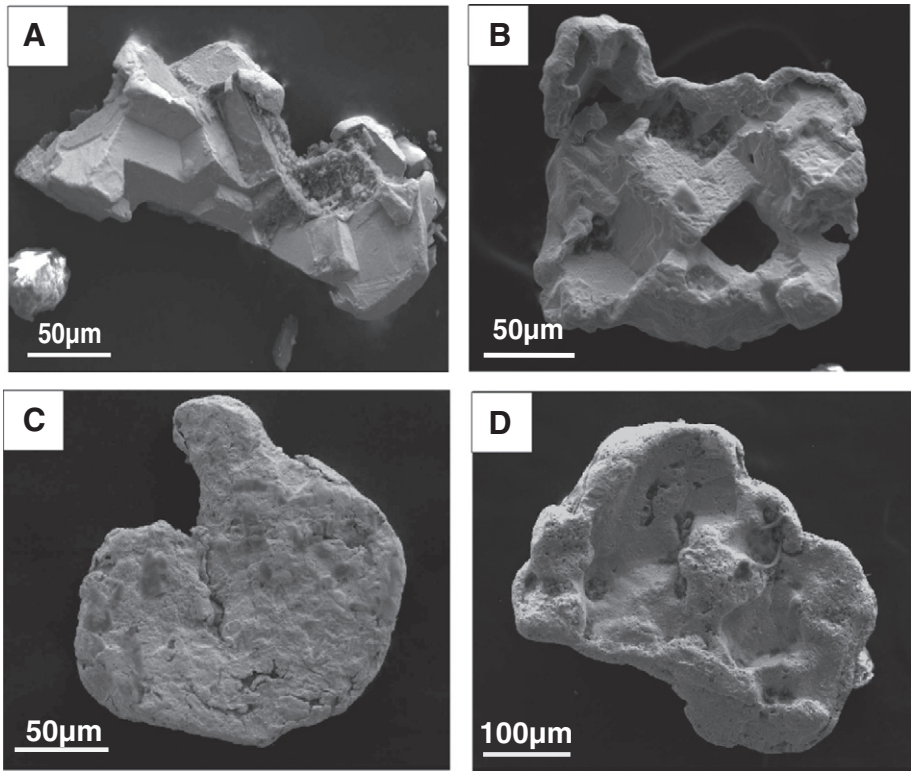

Fig. 9. SEM images of native gold grains in regolith material and karst: A. residual gold particle with prints of mineral grains from primary ores; B–D. gold particles with an increasing degree of supergene alterations (development of high-grade shell, corrosion).

Ag, Cd-containing tetrahedrite, zinkenite, and Pb-Cu-As-S phase), tellurides (hessite, tellurobismuthine), as well as barite and carbonaceous compounds (bitumens) (Fig. 10A–E).

The Auger spectroscopy data (Fig. 10F, G), obtained during layer-by-layer ion etching of the surface of cubic pyrite grains from the argillic zone, have shown: 1) an abnormally high carbon content on the surface of the grains (more than 55 at.%) slightly decreasing inward of the grains; 2) presence of nitrogen in some grains; and 3) individual grains show a deviation in S/Fe values from pyrite stoichiometry toward sulfur deficiency, which may be due to the formation of pyrrhotite-like phases on the pyrite surface by a mechanism discussed in Tauson et al. (2011).

Native gold in zones of clayey regoliths is attributed mainly to the fine (0.1 mm) and very small (0.1–0.25 mm) grain-size class. The gold particles have a different morphology (Fig. 11A–C). In some cases, such particles are overgrown by fine-grained aggregates of rounded microcrystals of a newly formed ("spongy") gold (Fig. 11F, G). The size of individual gold microcrystals in such aggregates does not exceed 5 μm, typically less than 1 μm. Finally, the particles composed of aggregates of small gold crystals containing inclusions of pyrite, quartz, grey ores, and hessite, were found (Fig. 8D).

In general, gold from clayey regoliths (saprolite) is characterized by large variations in fineness from <500 to 950–990. We found the particles represented by overgrowth of grains of different fineness from electrum to high-grade gold (Fig. 11E). The microcrystals of the newly formed "spongy" gold are predominantly of high fineness. In addition to silver, gold also contains 0.7 wt.% Cu and up to 5.5 wt.% Hg (Table 2).

7. Organic matter in rocks and ores

To detect and determine the types of organic matter, differential thermal analysis (DTA) in combination with thermogravimetry (DTG) was used. Results of these analyses are reflected on the DTA and DTG graphs. The most important diagnostic features of studied organic matter are exo-peak temperature and initial burn-off temperature (Volkova, 1990). The total loss on burnout (according to DTG) corresponds to the quantity of organic matter in a sample. The analysis showed that the organic matter in all samples refers to lower-middle kerite (initial burn-off temperature is around 200 °C). Also, according to exo-peaks on the DTA graph (T = 300–370 °C) organic matters are slightly altered and comparable to regional epigenesis level of alteration (lower than catagenesis facies). Phases of free carbon (graphite, non-structured carbonaceous material) and solid bitumen were not found, which proves a relatively low content of organic carbon in the rocks (from ≤0.05 to 0.75 wt.%).

Results of IR and NMR spectroscopy indicated that the composition of bitumoids is dominated by hydrocarbons of aliphatic series (Fig. 12). The various oxygen-bearing complexes are minor; their content variations reflect the degree of oxidation of organic matter. This parameter is independent of the rock type, but is variable in space. In particular, in the northern part of the deposit, the organic matter is oxidized from weak to moderate degrees. In the southern part of the field, the oxidation degree of organic matter is higher, and it is represented not only by complex ethers, but also by carboxylic acids. Multi-element and organometallic compounds containing halogens, N, O, P, F, B, and Si, have been determined in most geochemically active hexane fraction of bitumen from the limestone breccia using the method of gas chromatography-mass spectrometry. Sulfur- and metal-organic compounds were not found.

8. Geochemistry of ore and altered rocks

8.1. Elements associated with gold

The major mineralization elements are Au, As, Ag, Hg, Ba, Mn, Sb, Pb, Cu, and Zn to a lesser degree. The largest and most contrasting halos of these elements are confined to the contacts between volcano-sedimentary and carbonate strata and coincide with the position of the orebodies (Fig. 13). The occurrence of an aureole zone westward is

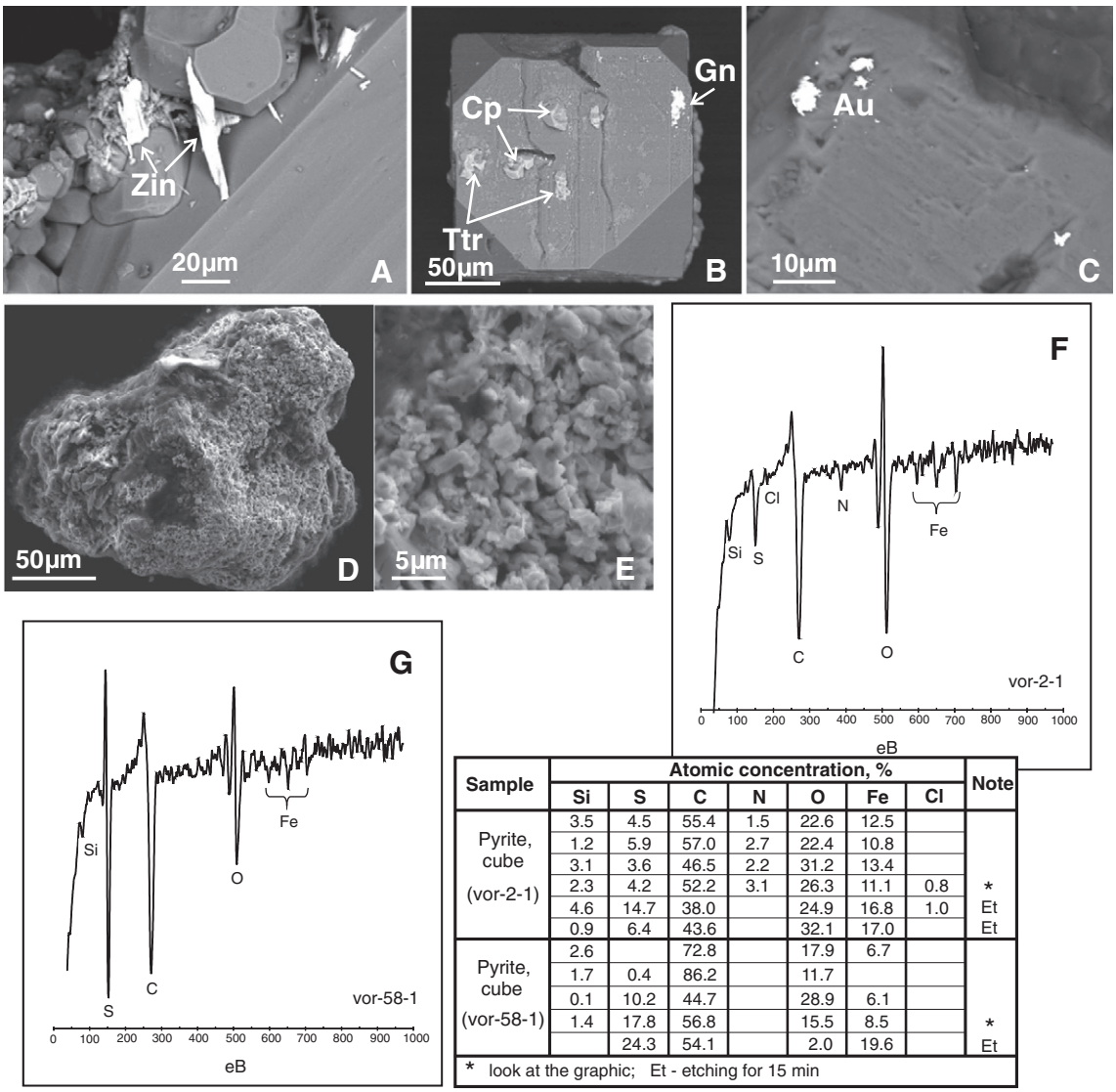

Sample	Atomic concentration, %							Note
	Si	S	C	N	O	Fe	Cl	
Pyrite, cube (vor-2-1)	3.5	4.5	55.4	1.5	22.6	12.5		
	1.2	5.9	57.0	2.7	22.4	10.8		
	3.1	3.6	46.5	2.2	31.2	13.4		
	2.3	4.2	52.2	3.1	26.3	11.1	0.8	*
	4.6	14.7	38.0		24.9	16.8	1.0	Et
	0.9	6.4	43.6		32.1	17.0		Et
Pyrite, cube (vor-58-1)	2.6		72.8		17.9	6.7		
	1.7	0.4	86.2		11.7			
	0.1	10.2	44.7		28.9	6.1		
	1.4	17.8	56.8		15.5	8.5		*
		24.3	54.1		2.0	19.6		Et

* look at the graphic; Et - etching for 15 min

Fig. 10. Pyrite from clay-altered rocks in a deep karst zone (type C2 ore). A–E. Newly formed sulfides on the surface of "fresh" pyrite grains: A. zinkenite, $PbSb_2S_4$ (Zin); B. (Ag, Zn)-bearing tetrahedrite (Ttr), galena (Gn), chalcopyrite (Cp); C. particles of high-fineness native gold (Au) on the surface of pyrite grains; D, E. partially oxidized pyrite grains of early generation overprinted by newly formed galena: general view (D) details of the galena aggregates (E); F, G. examples of Auger spectra of the surface of cubic pyrite grains and elemental composition of the face surface (Table).

controlled by the Vorontsovsky fault, elsewhere one can only observe low As and Ba halos, confined mainly to the karst deposits. In general, the elements aureole is controlled by zones of increased permeability for hydrothermal solutions, mylonitization and cataclasis, the appearance of dikes and brecciated limestones.

8.2. Trace element composition of country rocks

The trace element composition of representative samples of silicate ores in tuffaceous siltstones (type A3), together with carbonate and limestone breccias (type B1), is shown in Table 7. In general, the ores of these types differ slightly in their trace element content, which does not exceed 1–2 ppm for the following elements: Be, Ge, Se, Mo, Sn, Bi, Cd, Hf, Cs, Ta, U, Th, and REE (Sm, Eu, Gd, Tb, Dy, Ho, Er, Tm, Yb, Lu). On the other hand, concentration of up to a few tens of ppm is typical for Li, B, Sc, Y, Nb, W, Tl, Te, Ga, Co, Ag, Sb, Te, and REEs (La, Ce, Pr, Nd). Higher contents (up to 100 ppm) are established for Cr, Ni, Cu, Zn, Rb, Zr, Sb and Pb. The elements with the abundances higher than 100 ppm are Ti, V, Mn, As, Sr, Ba, and P. The carbonate ores relative to the silicate ones are distinguished by higher P, Ni, Sr, Sb and Te contents, and lower contents of As and Rb.

The total abundances of REEs in A3 and B1 ores vary from a few tens to 160 ppm and generally do not correlate with the degree of gold content. Chondrite-normalized REE patterns reflect the type of hydrothermal alteration in rocks and ores. Propylitized volcanic rocks are characterized by the simplest downward patterns, indicating LREE enrichment of these rocks with respect to the MREEs and HREEs (Fig. 14A).

Quartz-sericite alteration is superimposed on propylitically altered volcanic rocks, hosting the B3 ores. This alteration doesn't change the REE patterns, but it can be traced by a distinct negative Eu anomaly (Fig. 14B). A negative Ce anomaly appears additionally on the REE patterns of breccia cement, due to the presence of small fragments of limestone (Fig. 14C). Such REE patterns are also typical for the C1 ores (Fig. 14D). Previously we have also established that the total REE content in the Vorontsovskye carbonates increases from 3.7–5.6 ppm in the unaltered limestone of country rocks to 8.7–15.5 ppm in

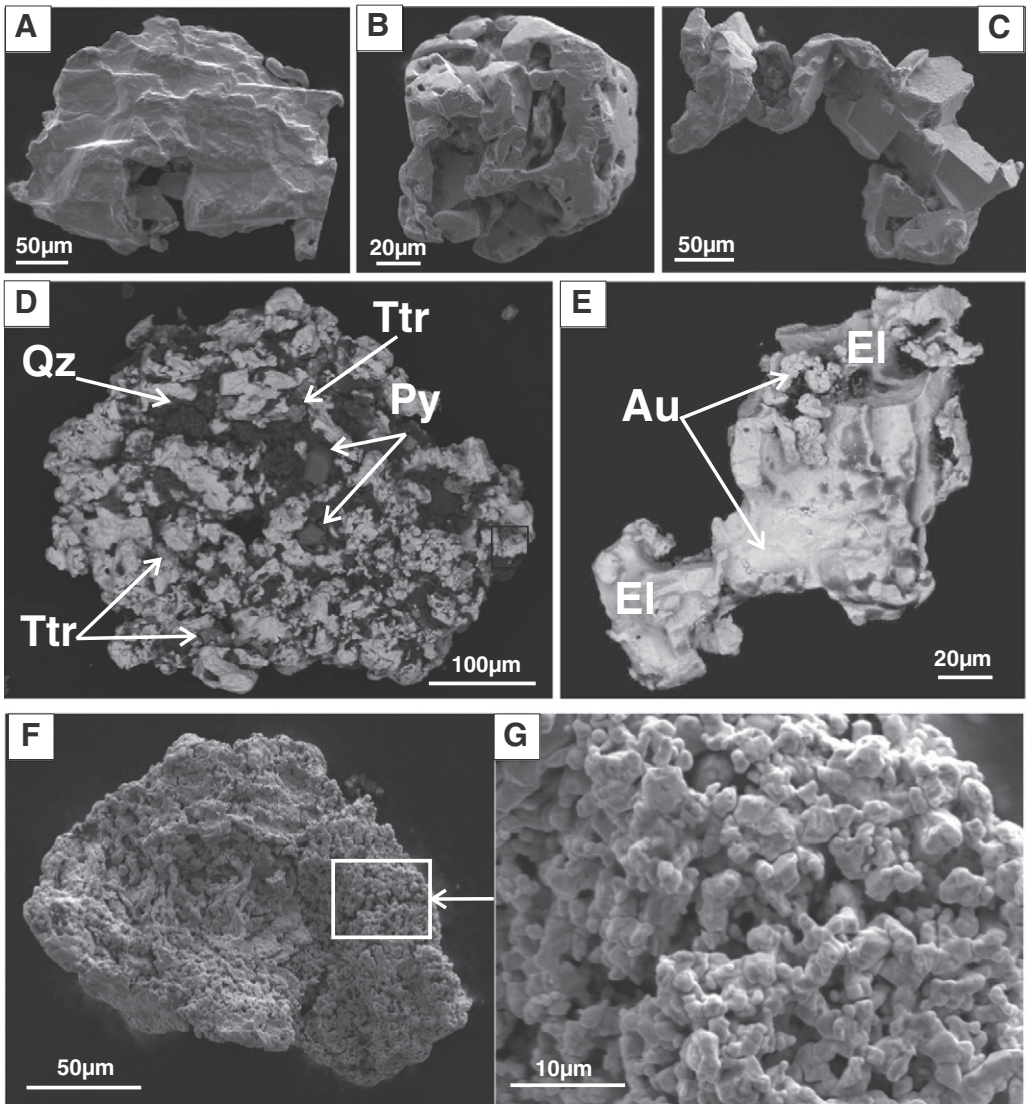

Fig. 11. Native gold from clay-altered rocks: A–C. characteristic gold typomorphs: lamellar (A) lumpy (B), a crystalline intergrowth of complex shape (C); D. high-fineness Hg-bearing gold aggregate (937–970‰, Hg-5.4%) in association with tetrahedrite (Ttr), pyrite (Py) and quartz (Qz); E. intergrowth between average fineness gold (Au) and electrum (El); F, G. overgrowth of flattened gold particle by newly formed gold aggregate: general view (F) and details of the aggregate structure (G).

recrystallized and marmorized limestone (Murzin et al., 2010). Carbonate of all ore-bearing formations (limestone breccia, jasperoids and skarns) contains even more REEs (21.8–54.8 ppm).

9. P-T-X conditions of ore formation

Assessments of temperature, pressure, and sulfur fugacity (P, T, fS_2) during formation of the main ore types were done using bicarbonate geothermobarometry, as well as thermometry based on the compositions of coexisting pyrite, pyrrhotite, and arsenopyrite, in particular, using the Co distribution between pyrite and pyrrhotite (Table 8). More detailed information about these methods was given earlier (Sazonov et al., 1991).

The early ore mineral assemblages were deposited at temperatures of 380 to 240 °C, whereas the late ones were deposited at lower temperatures ranging from 220 to 110 °C. The conditions of ore deposition in jasperoids (type A2 ores) were somewhat unstable. The process of ore deposition in jasperoids of both dolomite-ankerite and quartz facies began at 500–450 °C and hydrostatic pressure of 0.15–0.2 kbar, but a sharp increase in pressure up to lithostatic level (0.5–0.6 kbar) took place in the temperature range of 260–310 °C.

The decreased temperatures of deposition of the late productive ore assemblages of types A2 and B1 are confirmed by a thermo-cryometric study of the liquid-vapor inclusions in the carbonate of these ores (Naumov et al., 2001, 2002). The studied primary inclusions of 0.01 mm in size or less are located in the central parts of carbonate grains, and within growth zones of crystals. Two types of fluid inclusions are distinguished. The first type is prevalent and essentially has gas with liquid carbon dioxide, and the second is one- or two-phase with a filling close to 100%.

The presence of water and gas inclusions indicates a heterogeneous state of the fluid, determined during its boiling with a sharp pressure drop at near-surface conditions. For boiling phenomena, a requirement for trapping temperatures and homogenization temperatures is 110–150 °C, whereas for the paragenesis with realgar, the trapping temperature was less than 100 °C.

Cryometric studies of vapor inclusions of the first type showed that the gas phase contained an admixture of nitrogen or methane,

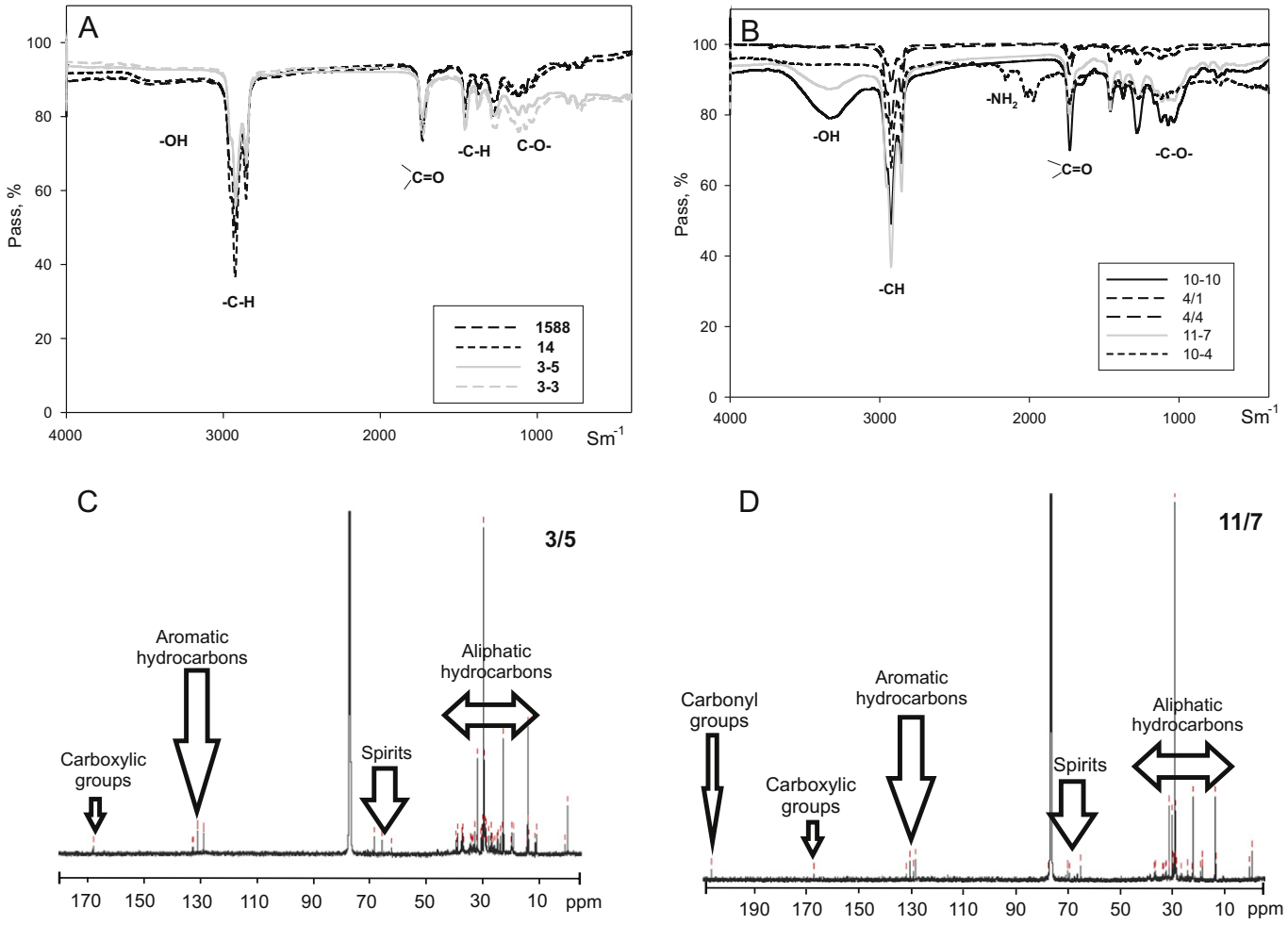

Fig. 12. Bitumen composition from different rocks at the Vorontsovskoe deposit, according to IR spectroscopy (A, B) and NMR-spectroscopy (C, D).

decreasing the melting point of CO_2 to −58 to −62 °C. The solutions of one- or two-phase inclusions point to the $CaCl_2$-H_2O-salt system, as evidenced by their eutectic melting point (−49 °C). The composition of solutions most likely contains NaCl and KCl, which is indirectly confirmed by sharp acceleration of ice melting at temperatures close to eutectics of the water-salt systems KCl-NaCl-H_2O (−23.5 °C) and KCl-H_2O (−10.6 °C). The total salt concentration in inclusion solutions, according to the melting point of ice of −4 to −6 °C, does not exceed 6.4–9.2 wt.% $NaCl_{eq}$.

10. Isotope systematics of minerals, rocks and ore-bearing fluids

10.1. The O, C and Sr isotopic compositions of carbonates

Our data on the isotopic composition of C and O at the Vorontsovskoe deposit (Sazonov et al., 1998; Murzin et al., 2010) were obtained from carbonate of the host limestone, and the carbonate formed during ore formation (Tables 9, 10), and briefly summarized here. It was established that the C and O isotopic compositions in the range of $\delta^{13}C$ = 1.3–2.3‰ PDB, $\delta^{18}O$ = 17.9–23.6‰ SMOW of limestone of hosting carbonate series corresponds to the rock reservoir of Phanerozoic marine carbonates (Fig. 15). Processes of limestone recrystallization, marmorization, and brecciation have little effect on the original isotopic characteristics of carbonate, which is expressed only in slight lessening of $\delta^{18}O$ with respect to the marine carbonate reservoir. In the process of gold-bearing ore formation at the Auerbah ore field, newly formed carbonate is characterized by a successive decrease of the carbon and oxygen isotopic compositions in a range: ore-bearing calcareous breccia-jasperoids-skarns-quartz veins. Fig. 16 shows that the Sr isotopic composition of carbonate also forms a single trend from a marine limestone to the mantle material in the same sequence of ore-forming processes.

10.2. Sulfur isotopic composition of sulfides

The sulfur isotopic data on igneous rocks at the Auerbah massif and sulfides at the Vorontsovskoe deposit are presented in Table 11 and in Fig. 17.

Sulfur of magmatic rocks and sulfides from the skarns (A1 ores) is close to the CDT value, but only slightly deviating from it in both the positive and negative areas, with $\delta^{34}S$ ranging from −2.9 to 2.7 and −1.2 to 0.2‰, respectively. The sulfur of pyrite, arsenopyrite, and stibnite from altered rocks (propylitic, sericitic, and argillic) and from A3 ores hosted by the volcanogenic part of deposit is lighter, with the $\delta^{34}S$ ranging from −1.8 to −4.6‰. Pyrite from volcano-sedimentary cement of calcareous ore-bearing breccia (B1 ores) contains even lighter sulfur with the $\delta^{34}S$ ranging from −0.4 to −7.8‰. Light S isotopic composition of sulfides points to the possible involvement of biogenic sulfur, which is confirmed by the presence of fine-globular pyrite relic in volcano-sedimentary rocks. Sulfides in jasperoids (A2 ores) (pyrite,

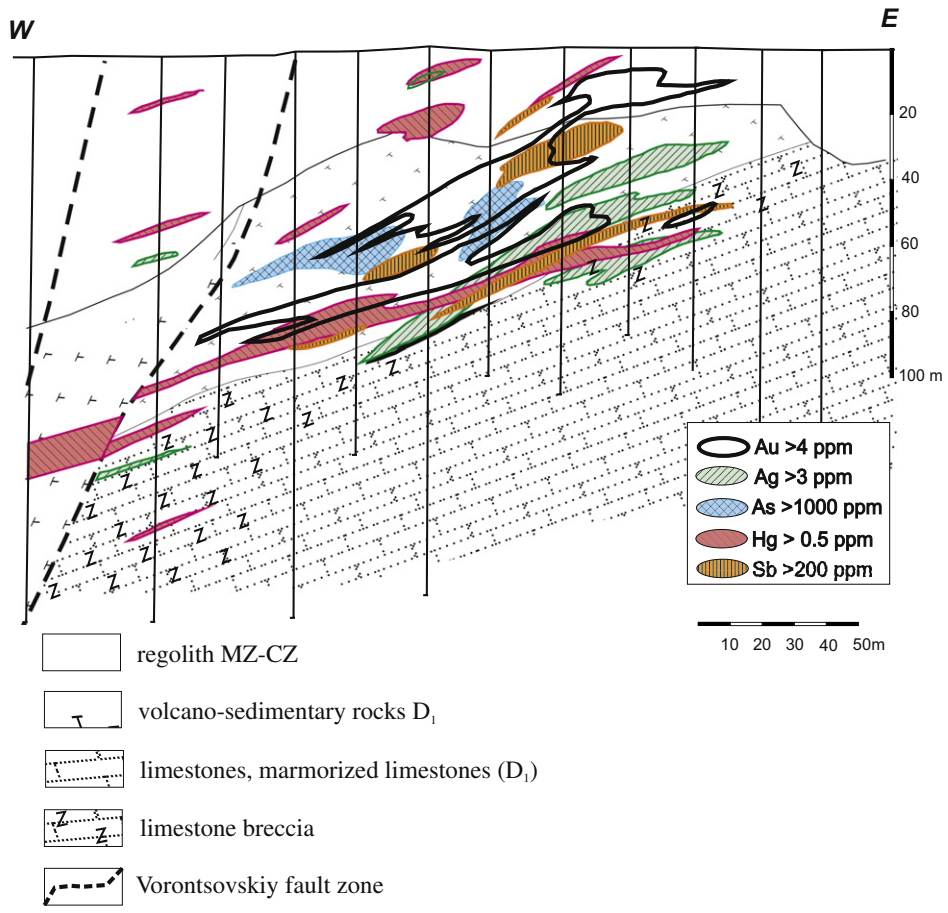

Fig. 13. Geochemical haloes of Au, Ag, Hg, As and Sb constructed along drill holes profiles through the central part of the deposit. Data from Vorontsovsky EMG.

sphalerite, and chalcopyrite) contain isotopically heavy sulfur ($\delta^{34}S$ from 1.6 to 4.5‰), which is probably due to the involvements of sulfate sulfur of silicified limestones. Extra heavy sulfur was also found in the sphalerite sample from quartz vein in granodiorite of the Auerbah massif of the Peschanskoye deposit.

11. Discussion

11.1. Age of mineralization and its relationship with magmatism

The position of the Vorontsovskoe deposit on the flank of the zoned volcano-plutonic complex together with the spatial superposition of gold and gold-bearing occurrences raises the issue of synchronicity of ore-forming processes and magmatism in the studied ore field.

Currently, there are several age data of igneous rocks from the Auerbah volcano-plutonic complex, which indicate comagmatic and synchronous formation of the Krasnoturyinsk volcanics and intrusive rocks of the Auerbah complex in the Lower Devonian. Krasnobaev et al. (2007) established the U-Pb age of zircon (using high-definition ion microprobe SHRIMP II) from quartz diorite at 404 ± 5 Ma (recrystallization age 384.5 ± 8 Ma) and from granodiorite at 393 ± 3.3 Ma (recrystallization age 285 ± 3 Ma). In general, Rb-Sr dating of igneous rocks (gabbro, gabbro-diorite, quartz diorite, granite) yielded the age of 405 ± 9 Ma, coinciding with the zircon dating of quartz diorite. Using the Sm-Nd (ID-TIMS) technique, Ronkin et al. (2009) obtained an age for biotite-pyroxene-amphibole diorites of 411 ± 25 Ma.

There is no consensus on the age of the Vorontsovskoe gold mineralization formation. Some researchers correlate the gold-arsenic mineralization to the intrusive magmatism, suggesting that the deposit is epi-mesothermal and distal to the porphyry-copper system. Minina (1994) noted that the porphyry diorite endocontact rim of the Auerbah intrusion is hosting the stringer-disseminated pyrite-chalcopyrite mineralization with elevated concentrations of gold and silver, as well as gold-bearing quartz veins. This author suggested that the deposits of Turinsk ore field are similar to skarn-type copper-porphyry deposits in the south-western USA, described by Einaudi et al. (1981). Although typical porphyry copper deposits are not present in the Turinsk ore field, Grabezhev et al. (2014) has reported the disseminated sulfides in diorites as porphyry Cu mineralization, first recognized in 1959–1962.

The U-Pb zircon dating (SHRIMP II) of quartz diorite, obtained by Grabezhev et al. (2014), yielded an age of 407.7 ± 1.6 Ma. This age was interpreted as an evidence that the formation of copper-skarn and porphyry copper mineralization is related to the quartz diorites, whereas iron-skarn mineralization was suggested to be related to the later granodiorites. Ugriumov (1993) also relates the gold mineralization to postmagmatic fluids, responsible for most of the metallic and nonmetallic components. Other researchers have suggested that the genetic link between the magmatism and gold-arsenic mineralization at the Vorontsovskoe deposit is due to the later events. Based on K-Ar dating of sericite from the cementing material of calcareous ore-bearing breccia (299 ± 8 Ma), Sazonov et al. (1991) correlate the gold-arsenic ores to the Carboniferous-Permian tectono-thermal events, caused by

Table 7
Trace element composition of silicate ores in tuffaceous siltstones (type A3), carbonate and limestone breccias (type B1), ICP-MS, ppm.

Element	A3 type (silicate ores in tuffaceous siltstones)					B1 type (ores in limestone breccias)			
Li	2.27	1.63	1.61	3.50	4.20	5.25	7.24	7.09	2.54
Be	0.20	0.12	0.22	0.26	0.42	0.24	0.15	0.30	0.12
B	1.93	3.94	1.86	5.75	14.31	0.38	7.15	3.02	1.78
P	547	538	599	517	524	1128	1337	801	2342
Sc	10.55	6.46	8.51	11.49	18.74	9.63	7.18	17.47	5.34
Ti	1743	1043	1412	1523	1924	1233	697	2239	1115
V	117.5	81.1	93.3	111.0	195.8	91.8	61.9	167.5	74.4
Cr	18.2	62.5	69.5	24.6	39.0	12.2	15.8	35.3	13.3
Mn	1663	679	1831	1063	132	30,802	20,944	461	226
Co	11.1	8.1	22.3	11.4	21.2	45.0	13.5	18.7	10.9
Ni	6.6	8.9	10.7	7.2	21.9	100.6	39.9	27.8	32.0
Cu	32.2	32.1	31.1	102.9	62.3	33.0	31.5	87.9	33.6
Zn	49.07	26.95	401.21	120.09	51.88	145.66	85.56	92.07	150.06
Ga	10.91	8.77	12.91	11.33	15.65	5.28	5.27	10.40	4.68
Ge	0.55	0.60	0.64	0.64	0.40	0.28	0.21	0.27	0.18
As	3381	946	371	6293	2718	419	105	422	286
Se	0.20	0.57	0.30	0.29	0.39	0.79	1.80	1.15	1.23
Rb	123.5	76.1	32.5	109.6	64.7	23.8	4.3	39.2	14.5
Sr	137	82	112	69	156	265	321	128	199
Y	10.8	5.9	10.6	10.2	11.0	20.3	14.1	12.0	29.6
Zr	36.7	33.8	40.1	40.3	56.1	17.5	10.5	35.1	16.1
Nb	0.96	0.81	1.08	0.94	1.88	1.72	0.45	1.18	1.47
Mo	0.26	0.41	1.13	0.57	0.56	5.37	1.53	0.71	3.03
Ag	2.24	11.07	3.06	4.01	0.21	1.51	29.28	0.18	0.14
Cd	0.16	0.14	1.36	0.46	0.19	1.32	0.85	0.85	2.48
Sn	0.39	0.37	0.47	0.45	0.76	0.67	0.23	0.84	0.77
Sb	45	39	91	131	30	114	701	107	87
Te	1.22	4.48	0.98	2.34	1.50	0.80	1.86	6.09	2.05
Cs	2.15	1.63	0.97	2.96	3.17	1.79	0.59	2.12	0.58
Ba	918	1788	488	427	1213	1366	47	1727	665
La	7.16	7.29	14.76	11.01	12.01	25.06	11.16	9.70	49.77
Ce	15.27	13.54	26.39	21.04	22.27	22.33	12.89	14.72	46.08
Pr	2.11	1.80	3.11	2.61	2.87	4.11	2.26	2.13	7.73
Nd	9.16	7.19	12.39	10.21	11.49	16.14	9.26	8.81	32.34
Sm	2.17	1.36	2.53	2.13	2.47	3.05	1.73	1.96	5.79
Eu	0.49	0.24	0.74	0.50	0.54	0.85	0.48	0.54	1.30
Gd	1.96	1.06	2.24	1.90	2.23	3.13	2.04	1.94	5.46
Tb	0.30	0.16	0.33	0.29	0.34	0.40	0.26	0.31	0.72
Dy	2.10	1.06	2.13	1.95	2.30	2.51	1.65	2.10	4.37
Ho	0.45	0.24	0.44	0.42	0.45	0.54	0.37	0.45	0.88
Er	1.45	0.79	1.35	1.28	1.53	1.54	1.06	1.31	2.40
Tm	0.22	0.12	0.21	0.20	0.21	0.20	0.14	0.19	0.30
Yb	1.44	0.88	1.43	1.39	1.31	1.26	0.88	1.25	1.69
Lu	0.23	0.14	0.22	0.21	0.19	0.18	0.12	0.20	0.23
Hf	1.23	1.07	1.31	1.29	1.77	0.57	0.38	1.18	0.72
Ta	0.06	0.05	0.06	0.06	0.12	0.08	н/о	0.08	0.08
W	1.19	3.74	72.69	3.03	5.71	12.25	3.72	4.65	2.26
Au	1.49	1.60	1.37	1.51	3.47	1.06	1.57	1.72	1.51
Hg	0.12	0.69	1.59	0.09	1.29	–	–	17.98	0.11
Tl	5.7	22.1	3.7	5.5	216.1	27.3	0.5	99.2	62.9
Pb	11.4	16.9	10.9	70.0	15.9	13.4	208.1	11.3	41.6
Bi	0.09	0.15	0.05	0.01	0.23	0.17	0.13	1.08	3.45
Th	2.30	2.17	2.82	2.70	2.89	1.55	0.68	1.98	1.43
U	0.91	1.05	1.36	1.44	1.34	1.89	0.38	0.87	0.95
Sum REE	44.52	35.85	68.27	55.14	60.21	81.30	44.29	45.62	159.07

fluid inflow from the mantle. Other ideas on the formation of gold mineralization advocate the Late Paleozoic-Mesozoic, Mesozoic and even Late Mesozoic-Cenozoic tectonic events being responsible for the development of the hydrothermally altered rocks of the argillic and jasperoid types (Bobrov, 1991; Savelyeva and Kostromin, 1991; Begetnev, 1999; Barannikov and Ugrumov, 2003; Azovskova et al., 2013a,b).

The available age data on the Vorontsovskoe main ore types are poorly constrained because of the difficulty in separating mineral species for isotopic dating. We obtained the Ar-Ar age of the hydromica sample with a structural modifications $2M_1 + 1M$, extracted from the mica-carbonate veinlet, which is crosscutting the gold-bearing calcareous tuffaceous siltstone with disseminated pyrite (A3 ore type). For this sample, we were able to determine a reasonably reliable plateau with seven steps, which corresponds to more than 98% of the extracted ^{39}Ar (Fig. 18). The obtained age of 391.1 ± 4.9 Ma is coeval with igneous rocks of the Auerbah complex.

11.2. Hydrothermal alteration and ore formation

As discussed above, hydrothermally altered rocks of various temperatures and ages occur at the deposit: high-temperature skarns, high-medium-temperature epidote-chlorite (propylitic alteration), quartz-sericite, jasperoids, and low-temperature argillic alteration (Sazonov et al., 1991; Sazonov, 1998; Sazonov et al., 1998). In addition, recent studies have established a carbonaceous type of low-temperature

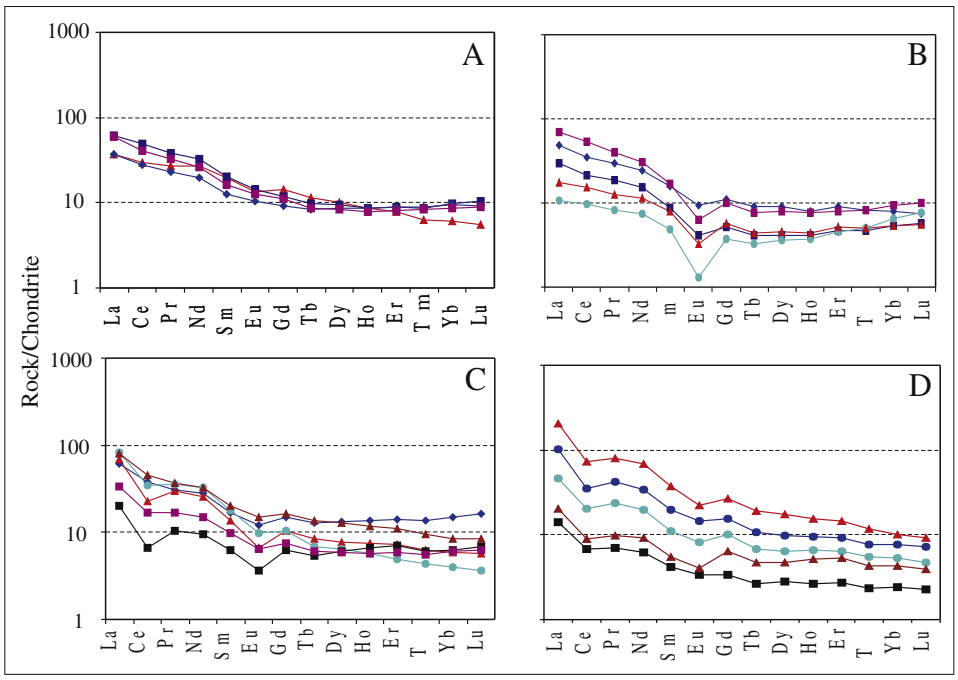

Fig. 14. Chondrite-normalized REE patterns of representative samples of altered rocks and ores from the Vorontsovskoe deposit. A. Propylitic tuffaceous siltstone, B. silicified and sericitized tuffaceous siltstone (type B3 ore), C. cement of calcareous breccia, D. calcareous breccia (type C1 ore).

bitumen alteration, which overprints all earlier alteration assemblages (Azovskova et al., 2013a,b).

Skarns and quartz-carbonate-sericite alteration are widespread outside the economic ore zones of the Vorontsovskoe deposit. These alteration systems, as well as deposition of gold and sulfides at the final stages of skarn formation, have a spatial and probably genetic link with the Auerbah volcano-plutonic complex (Murzin and Sazonov, 1996). Skarns and listvenites occur locally in the deposit and cross-cut by quartz vein, and possibly also related to the same complex formation. The relationships with other types of metasomatic rocks and ores were not reliably established. Propylitic alteration affects intermediate to felsic dikes, volcano-sedimentary rocks and the cement of calcareous breccia. Gold content in propylitized dikes is low (less than 0.2 ppm), even in the absence of disseminated pyrite. The degree of gold mineralization of the propylitized volcano-sedimentary rocks is uncertain, because the high Au concentrations coincide with zones of silicification and sericitization. At the Carlin deposit in the USA, all the above listed hydrothermal processes have not been developed, however, they do occur in other deposits of the Carlin trend and are considered in the model reported by Berger and Bagbby (1993).

Jasperoids are associated with silicification and dolomitization of carbonate rocks. They are considered to be formed under P-T-X conditions corresponding to listvenite, quartz-sericite and argillic alteration (Sazonov, 1998). At the Carlin deposit, a progressive silicification of carbonate rocks takes place in the following order: from the early decalcification (less than 100 °C) to argillic alteration (150–200 °C) and eventually to the formation of jasperoids (over 200 °C) (Radtke, 1985). The syn-ore alteration is represented by argillization and, to a lesser extent, silicification and jasper formation. At the Vorontsovskoe deposit, jasperoids are poorly productive and developed as a result of temperature decrease from 500 up to 220 °C (Table 8) from the silica-rich fluids, moving along the contacts between volcanic rocks of intermediate-mafic composition and limestones (Sazonov et al., 1998).

Argillic alteration develops independently or as a part of the quartz-sericite assemblage. It is assumed that auriferous argillites might be quite common, as observed at the Carlin deposit, and preceded by quartz-sericite preserved in places as relics. Argillites locally occur in fault zones (Fig. 4), where they are not auriferous (Chekvaidze et al., 1995), and in gold-bearing karst regoliths (C2 ores). The latter are products of hypogene-supergene processes of Mesozoic age (Barannikov and Ugrumov, 2003; Azovskova et al., 2013a,b). Quartz-sericite altered rocks contain argillic-specific mineral parageneses which were formed at the final stages at lower temperatures below 220 °C. The Ar-Ar age of 391.1 ± 4.9 Ma was obtained for this stage was using hydromica.

Table 8
PT-conditions of formation of the main ore types in Vorontsovskoe gold deposit.

Ore type	Mineral assemblage	T, °C	P, kilobar	Log f_{S2}
A1	Pyrite-pyrrhotite–polymetallic	300 to 200	0.4 to 0.6	<−10
A2	Arsenopyrite-pyrite	450 to 240	0.15 to 0.20	−7 to −9
	Sulfosalts-polymetallic	260 to 220	0.5 to 0.6	
	Sphalerite-arsenopyrite-pyrite	510 to 300	0.15 to 0.20	−7 to −14
	Polymetallic	260 to 110	0.15 to 0.60	
A3	Pyrite-arsenopyrite	400 to 310	0.2 to 0.4	−7 to −10
B1	Pyrrhotite-arsenopyrite	370 to 300		−9 to −12
	Orpiment-realgar	250 to 150		

11.3. Organic matter in the ores

Organic matter is present at the Vorontsovskoe deposit similar to the Carlin-type deposits, where it is known as carbonaceous ore (Bagby and Berger, 1985; Cline et al., 2005). The content of organic matter in ores is less than 1 wt.% (Table 6), which is lower than that at the Carlin-trend deposits in the USA, but is comparable to equivalent ore deposits in China (Azovskova et al., 2011; Konstantinov, 2006; Rovnushkin and Azovskova, 2012). Analysis of available data shows that the ores of the mentioned deposits differ not only in the content of organic matter, but also on the forms of its occurrence, the time of occurrence relative to the period of ore deposition and, hence, its possible role in gold transportation or deposition.

The Carlin-type deposits of the USA are characterized by a wide range of organic species, from graphite to various bitumen types including their soluble forms. The occurrence of organic matter preceded ore formation, however, during hydrothermal processes it underwent remobilization into the fractures in the sedimentary rocks, into barite and quartz veins (Hausen and Kerr, 1968). Where the content of organic

Table 9
Isotopic composition of C, O and Sr of carbonates from Auerbah ore field.

Rock type	Sample, drill hole/deep	$\delta^{18}O$, SMOW	$\delta^{13}C$, PDB	$(^{87}Sr/^{86}Sr)_{norm}$
Vorontsovskoe gold deposit				
	670/390	21.2	1.9	
	666/343.7	21.0	1.6	0.707788 ± 7
Hosted limestone	751/176.5	21.5	1.4	
Recrystallized limestone	395/131	18.8	1.3	0.707355 ± 9
	606/111.3	17.9	1.7	
	903/80	23.4	1.6	0.707930 ± 6
	280/77.3	19.8	2.3	
	280/77.4	18.8	1.8	
	281/83.7	22.5	0.6	
	281/83.8	22.8	1.6	
	281/85.5	23.5	1.5	0.707819 ± 8
	281/85.6	23.6	1.7	
	670/224.2	23.1	1.4	
Limestone breccias (not gold-bearing)	670/269.7	16.9	1.8	
	670/269.8	16.8	1.7	
	666/257.7	18.0	−1.2	
	666/257.7	17.3	−2.6	0.707139 ± 11
	751/108	16.8	0.5	
	751/109	18.3	−0.1	
	748/63.5	19.3	1.9	
	748/63.6	17.4	−1.8	
	748/74	18.1	−0.3	0.707697 ± 10
	748/75	17.3	−0.2	
	275/118.6	16.6	1.8	
	276/151.2	18.1	2.1	0.707416 ± 8
	276/151.3	18.6	1.8	
	276/154	18.3	1.9	
	276/155	19.1	1.7	
Limestone breccias (gold-bearing, B1 ore type, hydrothermally altered)	276/156	18.3	1.8	
	21/121	19.8	2.1	
	276/170.8	22.7	2.1	0.707885 ± 6
	737-2[a]	17.1	−1.8	
	737-3	20.7	1.2	
	332/284.5[a]	16.2	−0.7	
Gold-bearing jasperoids (ore type A2)	332/286[a]	14.9	−4.3	0.704803 ± 6
	287/53.5	16.8	−2.1	
	396/84	13.4	−2.4	
	334/128.6	12.8	−4.0	0.706369 ± 7
Sulfidized skarn (ore type A1)	1001/95.0	12.2	−2.9	
Auerbah ore field, gold-bearing Cu-Fe skarn				
Vadimo-Alesandrovskoe Cu deposit	654	10.5	−7.0	
Vorontsovskoe Fe deposit	540	9.5	−5.6	
	962	10.0	−3.9	
North Peschanskoe Fe deposit	964	11.3	−3.5	
Auerbah ore field, gold-bearing veins				
	546	9.6	−6.3	
	844	9.5	−6.2	
	1-Pe(2)[a]	12.3	−7.1	
Peschanskoe Au deposit	1-Pe(1)[a]	11	−5	

[a] Dolomites, other samples - calcite.

matter is less than 3 wt.%, it directly correlates with Au-Hg-As-Sb, whereas higher contents correlate with Au-Hg (Konstantinov, 2006; Cline et al., 2005). It was also established that when the organic content is higher than 0.3 wt.%, most of the gold is associated with carbonaceous matter, likely in the form of gold-organic compounds represented by chelates (Radtke and Scheiner, 1970).

In the Carlin-type deposits in China (Golden Triangle; Pirajno, 2013), the organic matter is represented mainly by bitumens, and to a lesser extent by graphite-like phases (Gu et al., 2012; Lu, 1994).

At the Vorontsovskoe deposit, the free carbon phase is absent and organic matter is represented by low-middle kerites, which are the least structurally ordered varieties in the kerite-anthraxolite-schungite-graphite series (Fig. 12). The alteration of organic matter is minimal and it is within the limits of regional epigenetic facies. We consider that organic matter in the ores from the Vorontsovskoe deposit is not genetically associated with the host sedimentary and volcano-sedimentary rocks, but, instead, it has an endogenous nature (Azovskova et al., 2011; Azovskova et al., 2013a,b). Its deposition occurred after the cessation of Paleozoic metamorphic and metasomatic processes and, most likely, preceded or was coeval with the appearance of argillization in the Mesozoic tectono-thermal event (Barannikov and Ugrumov, 2003). The currently available data do not allow us to confirm the genetic relationship between the organic matter and gold. The high carbon content on the surface areas of the pyrite crystals from argillic alteration associated with a variety of ore minerals (C2 ore) provides a basis for such assumption. Organic matter creates the reducing conditions favorable for deposition of native metals, including gold (Section 6.6).

11.4. Gold species

The ores at the Vorontsovskoe deposit contain almost all ore minerals typical of Carlin-type deposits. In both cases, the ores consist of finely disseminated pyrite and arsenopyrite, and minor Cu, Zn, Pb, As, Sb, Hg, and Tl sulfides. The most common gold-bearing mineral at the Carlin-trend deposits is arsenic-bearing pyrite. Pyrite grains vary in size from the few microns to a few hundred microns and contain 0.33–4.9 wt.% of As and up to 1465 ppm of Au (Wells and Mullens, 1973; Fleet and Mumin, 1997; Simon et al., 1999). Gold in arsenic-bearing pyrite occurs in isomorphic and native forms as nano-size particles in various proportions. Several mechanisms of native gold occurrence were proposed: during co-crystallization with pyrite, if the solubility limit of isomorphous gold in arsenic-bearing pyrite is exceeded; or as a result of its separation from the pyrite matrix at the late stages of ore process (Palenik et al., 2004; Reich et al., 2005).

At the Vorontsovskoe deposit, As is fixed only in pyrite of types A3 and B1 ores, and its content ranges from 0.05 to 0.40 wt.% (Tables 4, 5). This fact suggests that the content of isomorphic gold in these pyrites is relatively low. Nevertheless, the bulk gold in all ore types is represented by its native form in particles typically less than 10 μm in size, which occur among the non-metallic minerals and, rarely, in sulfides. The composition of native gold in type C2, A1, and A2 ores is characterized by wide variations in fineness (610–990) and occasional presence of Hg impurities (up to 5.5 wt.%). In contrast, type A3 and B1 ores contain gold particles of high fineness varying in a narrow range of 930–1000 and with constant Hg admixture up to 3.5 wt.% (Table. 2).

The features of pyrite and gold speciation in the ores of the Vorontsovskoe deposit appear to be related to higher temperatures of these minerals deposition. Whereas at the Carlin-type deposits Au-bearing arsenic pyrite was deposited at temperatures of 120–250 °C (Wells and Mullens, 1973; Reich et al., 2005), at Vorontsovskoe deposit it was deposited above 300 °C (Table 8).

11.5. Sources of ore materials and ore-bearing fluids

Our data suggest heterogeneity of the source materials and ore-bearing fluids involved in formation of various ore types at Vorontsovskoe deposit.

The bulk sulfur comes from a deep-seated igneous intrusion, which was responsible for the formation of skarn sulfides. The lighter sulfur isotopic composition of sulfides in ores of volcano-sedimentary rocks (type A3 ores) and in the cement of ore-bearing calcareous breccia (B1 ores) indicates a possible mixing of magmatic sulfur with biogenic sulfate-reduced sulfur, as evidenced by the presence of relict fine-globular pyrite in the volcano-sedimentary rocks. The heavier isotopic composition of sulfur during the formation of polymetallic ores in jasperoids (A2 ores) is probably related with the mixing of deep-seated magmatic sulfur with sulfate sulfur from limestone replaced by quartz. The deep-seated sulfur reservoir dominated only during the formation of skarn ore sulfides (type A1).

Table 10
H_2O and CO_2 isotopic compositions of host rocks and minerals from fluid inclusions and calculation of the isotopic composition of the fluids that formed the Vorontsovskoe Au-Hg-As deposit.

Rock, host mineral (number of analyzed samples)	Isotopic composition of minerals			Calculated isotopic composition of the fluid, ‰			
	δD, ‰ SMOW	$\delta^{13}C$, ‰ PDB	$\delta^{18}O$, ‰ SMOW	T calc., °C	$\delta^{13}C$ (CO_2)	$\delta^{18}O$ (CO_2)	$\delta^{18}O$ (H_2O)
Ore breccia without realgar, calcite (4)	–	−0.1 to −2.6	17.3 to 18.3	370 to 300	−0.6 to 2.5	25.3 to 27.1	11.5 to 14.1
Ore breccia with realgar, calcite (6)	–	1.7 to 2.1	16.6 to 19.1	250 to 150	1.9–3.4	26.0 to 29.8	3.5 to 11.6
Jasperoid, dolomite (4)	–	−0.7 to −4.3	14.9 to 17.1	380 to 220	1.3 to −3.6	22.6 to 26.7	4.9 to 13.0
Jasperoid, quartz (3)	–	–	13.9 to 15.6	300 to 200	–	–	2.3 to 8.6
Jasperoid CO_2 from fluid inclusions in the quartz (3)	–	–	–	–	−2.8 to −3.2	–	–
Jasperoid, H_2O from fluid inclusions in the quartz (3)	−53 to −74	–	–	–		–	–
Fe-Cu skarns, calcite (7)	–	−2.4 to −7.0	9.5 to 13.4	400 to 200	0.3 to −6.8	17.1 to 23.5	−0.3 to 9.8
Quartz veins, dolomite (4)	–	−5.0 to −7.1	9.5 to 12.3	300 to 200	−3.7 to −7.9	15.5 to 22.3	−0.5 to 6.3

Notes: To calculate ^{13}C (CO_2) in carbonate, we used isotopic equilibrium calcite-dolomite-of CO_2 and CO_2 (Ohmoto and Rye, 1979). To calculate the $\delta^{18}O$ (CO_2), we used isotopic equilibrium calcite-CO_2 and CO_2-dolomite (Zheng, 1999). To calculate the $\delta^{18}O$ (H_2O), we used isotopic equilibrium calcite-water, water-dolomite (Zheng, 1999) and quartz-water (Zheng, 1993).

To determine the sources of carbon dioxide and water, we obtained their isotopic characteristics calculated on the basis of O and C isotope fractionation factors between fluid and equilibrated carbonate and quartz at 150–400 °C (Table 10). In addition, we used direct determination of the isotopic composition of carbon dioxide and hydrogen of water from the gas-liquid inclusions in quartz of three jasperoid samples.

Our calculations show that the quartz-sericite altered rocks and gold-arsenic ores of type B1 were formed from the fluids with carbon dioxide isotopic composition close to that of marine limestones ($\delta^{13}C_{CO}$ in a range from −0.6 to 3.4‰ and $\delta^{18}O_{CO2}$ in a range from 25.3 to. 29.8‰), The oxygen isotopic composition of water from fluid responsible for early high-temperature mineral assemblage deposition is in a range from 11.5 to 14.1‰ ($\delta^{18}O_{H2O}$), which is heavier than that in the magma source ($\delta^{18}O_{H2O}$ 6 to 10‰; Faure, 1986) and corresponds to metamorphic water. During the deposition of late low-temperature C1-type ore assemblage, $\delta^{18}O_{H2O}$ isotope values of water vary from 3.5 to 11.6‰. Therefore, the ore-forming fluid has equilibrated with marine sediments.

Fluid responsible for the formation of jasperoids of type A2 ores is characterized by carbon dioxide with the calculated $\delta^{13}C_{CO2}$ values of −3.6 to 1.3‰. This carbon dioxide has a lighter C isotope composition in comparison to that of above-mentioned values for B1 types ores, approaching juvenile C (−4 to −6‰; Faure, 1986). The analytical estimates (−2.8 to −3.2‰) in carbon dioxide, extracted from gas-liquid inclusions, fall within the range of calculated $\delta^{13}C_{CO2}$. At the same time, the $\delta^{13}C_{CO2}$ values of the fluids during the formation of jasperoids (from 22.6 to 26.7‰) are characterized by heavy O, as that for type C1 ores, i.e. corresponding to the O isotopic composition of marine limestone. The calculated O isotopic composition of water (2.3 to 8.6‰) is close to the $\delta^{18}O_{H2O}$ values of water of the magma source with 5–10‰ (Faure, 1986).

The lightest isotope characteristics are peculiar to hydrothermal solutions that formed A1-type skarn ores ($\delta^{13}C_{CO2}$ ranging from −6.8 to. 0.3‰, $\delta^{13}C_{CO2}$ from 17.1 to 23.5‰ and $\delta^{13}C_{H2O}$ from −0.3 to 9.8‰). Quartz veins in the Auerbah intrusion and its exocontacts have the following isotopic values of $\delta^{13}C_{CO2}$: from 7.9 to −3.7‰, $\delta^{13}C_{CO2}$ from 15.5 to 22.3‰ and $\delta^{13}C_{H2O}$ from −0.5 to 6.3‰. These values of C and O isotopic compositions probably resulted from the exchange between the post-magmatic fluids and limestones.

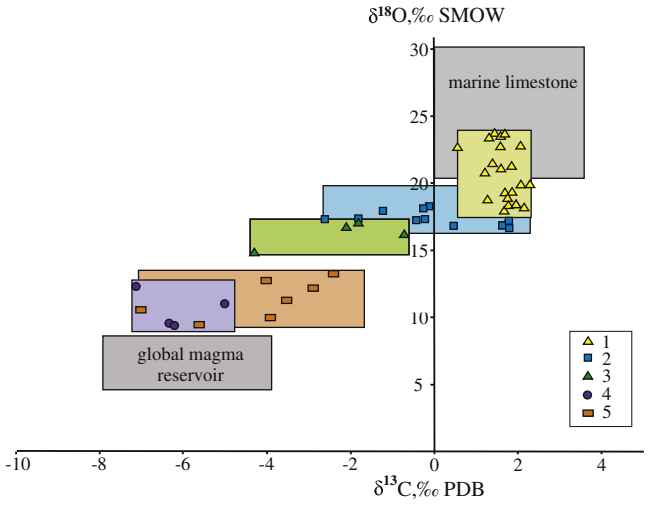

Fig. 15. Diagram of C and O isotope ratios in carbonates at the Vorontsovskoe deposit. (1–3) and Auerbah ore field (3.4): 1. limestone and marmorized limestone; 2. ore-bearing calcareous breccia; 3. jasperoids; 4. Cu-Fe-skarns; 5. quartz veins. The fields of global magma reservoir and carbonate from marine limestone are also plotted on the diagram.

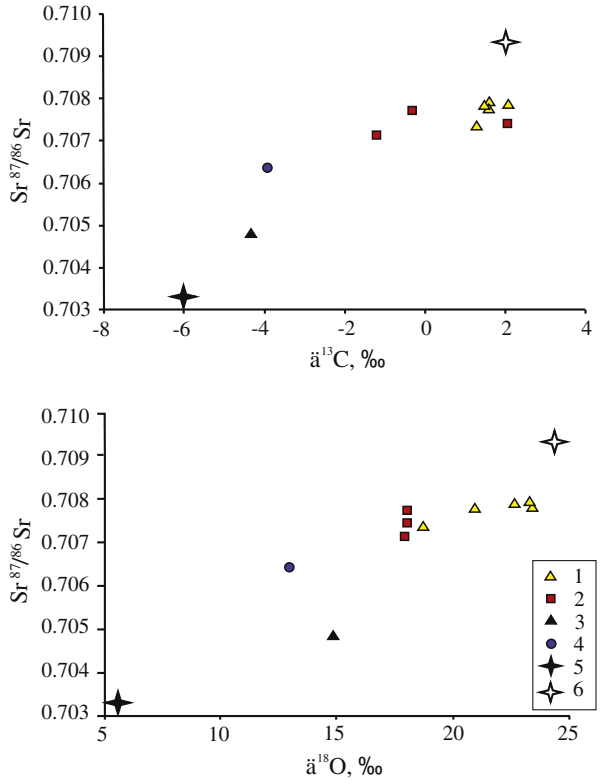

Fig. 16. Relationships between the C, O and Sr isotopic compositions of carbonates from the Vorontsovskoe deposit. 1. Limestone of host rocks and fragments of calcareous breccia, including recrystallized and marmorized limestones, 2. carbonate from cement of ore-bearing calcareous breccias, 3. jasperoidal carbonate, 4. calcite of skarns, 5. global mantle reservoir, 6. marine limestone.
After Murzin et al. (2010).

Table 11
Isotopic composition of S from magmatic rocks of Auerbah magmatic complex and from sulfide minerals of Vorontsovskoe Au deposit.

Sample	Rock type	Mineral	δ^{34}S. CDT
Magmatic rocks of Auerbah magmatic complex			
209/37.05	Quartz diorite		−2.9
224/46	Diorite		−2.4
326/52.1	Andesite porphyrite		−0.9
282/27	Gabbro		2.7
335/166	Andesite basalt porphyrite		−0.4
355/48	Basalt porphyrite		−0.3
Vorontsovskoe Au deposit			
1001/95	Sulphides from gold-bearing skarn (ore type	Chalcopyrite	−0.4
396/84.0	A1)	Pyrrhotite	−1.2
397/84.0		Chalcopyrite	−1.1
396/84.0		Pyrite	−1.1
396/87.6		Pyrite	−1.2
334/95.8		Pyrite	0.2
296/113.0		Sphalerite	−0.2
702/155.3	Jasperoid (ore type A2)	Sphalerite	2.6
332/284.5		Pyrite	4.5
332/284.6		Chalcopyrite	2.5
287/53.5		Pyrite	2.8
334/128.6		Sphalerite	1.6
276/97.5	Tuff siltstone (ore type A3)	Pyrite	−2.3
201/86.5	Limestone breccias (ore type B1)	Pyrite	−4.2
347/50		Pyrite	−7.2
347/70.5		Pyrite	−7.8
600/226		Pyrite	−0.4
1/1-K	Gold-bearing argillizite (ore type C2)	Pyrite	−2.1
1/1-C		Pyrite	−2.0
1/4		Pyrite	−1.8
2/1-K		Pyrite	−3.0
2/1-C		Pyrite	−3.0
1/2		Arsenopyrite	−1.9
1/3		Arsenopyrite	−3.5
1/5		Stibnite	−4.6
Peschanskoe gold lode deposit			
843	Quartz lode	Sphalerite	5.1

The presence of two isotopic reservoirs of water and carbon dioxide suggests that metamorphic fluid has equilibrated with limestone and magmatic fluids, mixing in various proportions, as observed by correlating trends of C, O, and Sr isotopes (Fig. 16).

11.6. Genetic models

11.6.1. Carlin-type deposits

Currently, there is no well-established genetic model for the formation of Carlin-type deposits. One of the first models was proposed by Radtke et al. (1980) and Radtke (1985) for the Carlin deposit in Nevada, USA. In this model, the mineralization was generated by hydrothermal processes activated by heat supplied by the Late Triassic intrusive rocks. Meteoric fluids were heated by igneous intrusions, reacting with rocks at a depth and extracting ore-forming components. The ore-forming fluids migrated along faults to the surface into the permeable rocks of Robert Mountains. Subsequent studies complicated the general concepts on the genesis of the Carlin-type mineralization. In what follows, we discuss the following models (Berger and Bagbby, 1993; Emsbo et al., 2003; Cline et al., 2005): 1) igneous, 2) metamorphic, 3) deep-seated circulation of meteoric water, and 4) polychronous remobilization.

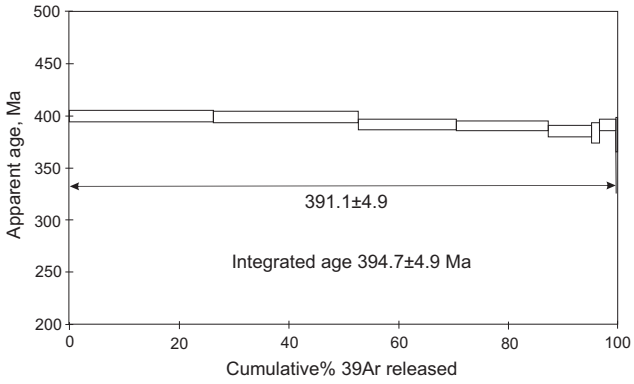

Fig. 18. ^{40}Ar/^{39}Ar plateau for sericite from the Vorontsovskoe gold deposit (sample Vr-10-12).

In the magmatic model, fluids, ore components including gold, and thermal energy for the transport of fluids to the surface are produced by magmas (Alvarez and Noble, 1988; Arehart et al., 1993; Sillitoe and Bonham, 1990; Ressel et al., 2000).

In the metamorphic model, fluids (H_2O, CO_2, H_2S) are generated as a result of prograde metamorphism of sedimentary rocks at depth under the influence of magmatism (Seedorff, 1991; Phillips and Powell, 1993; Groves et al., 1998). The fluids extract gold from the sedimentary rocks and transport the ores to the surface along faults.

The third model posits deep circulation of meteoric water during crust deformations as it extended through to the Cenozoic (Hofstra, 1994; Ilchik and Barton, 1997). Meteoric fluids penetrate to a depth of 10 km, where they extract gold and other ore components. Fluids discharge and ore formation occurs in the upper levels, where fluids react with the surrounding rocks. A somewhat similar concept was proposed by Craw et al. (2013), for the circulation of meteoric solutions along the Alpine Fault in New Zealand, their discharge at the surface as hot springs and the role of seismic pumping for the deposition of gold and other metals.

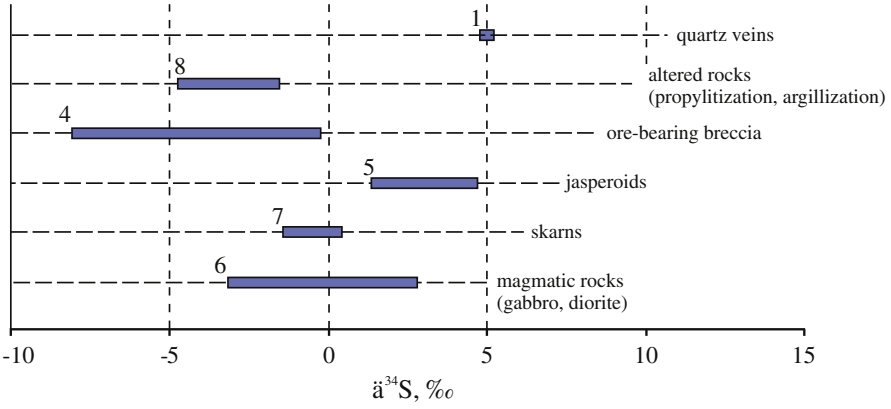

Fig. 17. Sulfur isotopic composition of the Auerbah igneous rocks and sulfides from various ore-metasomatic units of the Vorontsovskoe deposit. Numbers indicate the number of analyses.

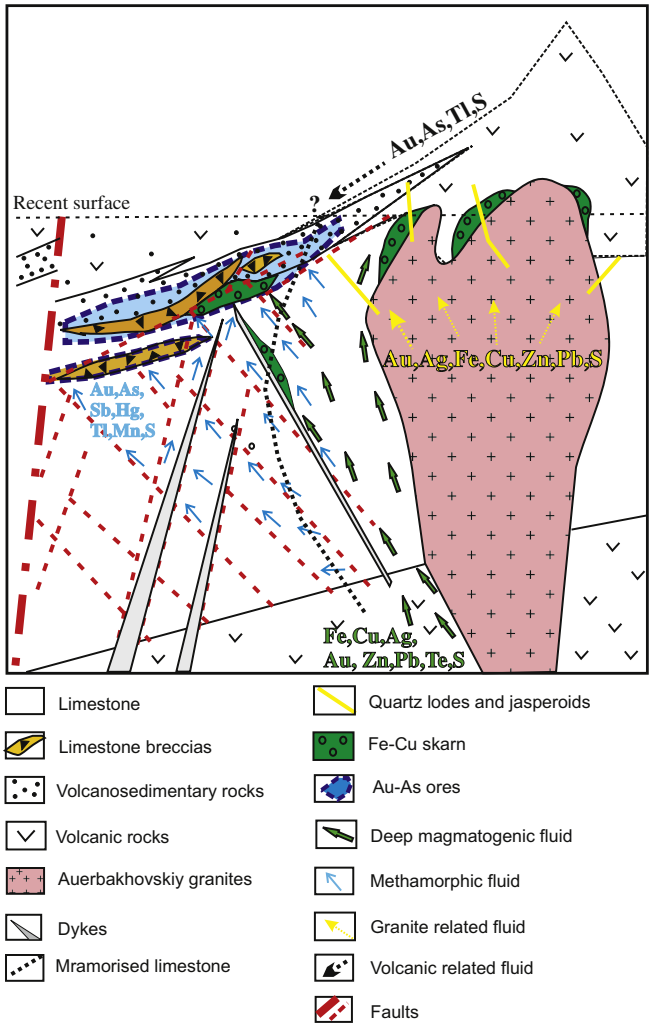

Fig. 19. Genetic model for the Vorontsovskoe Au deposit.

The fourth model is based on the study of deposits in the northern part of the Carlin trend (Emsbo et al., 2003). It proposes the existence of an intermediate source of gold and associated elements (As, Sb, Hg, Tl, and Ag), represented by SEDEX-type Devonian deposits. Remobilization of metals from the early intermediate source by hot meteoric waters would have occurred in Mid-Cenozoic time.

In addition to the above-mentioned genetic models of Carlin-type mineralization, there are other models, which are poorly substantiated. In particular, these include the concept of a leading role of ore-bearing mantle fluids, represented by a mixture of organometallic compounds and inorganic metal complexes (Zubkov, 2000). This fluid ascends from the mantle along the deep faults zones under non-equilibrium conditions. Also poorly substantiated are the concepts on formation of ores as distal low-temperature analogs of auriferous skarns (Sawkins, 1984) as distal meso-epithermal of copper porphyry systems (Minina, 1994; Grabezhev et al., 2014), and as regenerated primary sedimentary deposits (Bakulin, 1998).

11.6.2. Proposed genetic model for the Vorontsovskoe Au-Hg-As deposit

Our data do not allow us to ascribe the conditions of the Vorontsovskoe deposit formation to any of the above-mentioned models for a Carlin-type mineralization. However, some features of these models can be applied to the Vorontsovskoe deposit.

In our opinion, a suitable model for the genesis of the Vororontsovskoye deposit would involve four stages combining the participation of metamorphic and magmatic fluids (Fig. 19). Stage 1 implicates the formation of tuffaceous rocks, calcareous breccia horizons, extensional tectonics and intrusions of diorite porphyry dikes. The heating of the sedimentary and volcano-sedimentary rocks resulted in the release of metamorphic water which extracted ore components, including gold. However, the involvement of an exhalative-sedimentary transport of fine gold particles with their subsequent burial in tuffaceous sedimentary rocks is not ruled out.

Stage 2 is characterized by: (i) intense shearing and jointing, (ii) the intrusion of igneous rocks, (iii) mixing and equilibration of magmatic fluids and water from the zone of contact metamorphism of volcano-sedimentary rocks, (iv) extraction of metals and metalloids, particularly As, and (v) movement of metamorphogenic solutions along the margins of a core complex. The contact zones and the highly permeable breccias in limestones served as a focus and discharge zone for solutions responsible for the formation of Au-As ores of types A3 and B1, carrying the bulk of the gold in the deposit.

In Stage 3, there was an inflow of fluids carrying Fe, Cu, Zn, Pb, Ag, Au, Te, and S from deep-seated intrusions. Discharge of fluids in carbonate rocks generated the jasperoidal type A2 ores, whereas auriferous skarns with type B1 ores formed along the contacts between sedimentary rocks and the intrusions. Skarn-generating solutions penetrated along faults and the dike contacts, resulting in distal skarns, with no visible association with granitic intrusions. Finally, magmatic fluids from the cooling magma entered the Auerbah massif and in its exocontact sectors, resulting in the formation of listvenites and associated quartz veins, which locally replace the skarns.

These features are overprinted by low-temperature argillic and bituminous alteration over the Mesozoic regolith material (type C2 ores), belonging to the 4th stage of mineralization. These saprolitic rocks in the Urals are considered by some researchers as being of a mixed "hypogene-supergene" nature (Barannikov and Ugrumov, 2003). They originated under the conditions of a large-scale peneplanation as a result of the cumulative effect of arising juvenile hypogene solutions (mineralized thermal waters) and descending supergene highly-reactive meteoric waters.

12. Conclusions

A number of geological, geochemical and mineralogical features suggest that the Vorontsovskoe deposit has some characteristics of the Carlin-type mineral systems. These features include: 1) association of mineralization with volcano-sedimentary rocks, dominated by limestones; 2) stratiform nature of the orebodies and the mineralization being sited along tectonic contacts between volcano-sedimentary rocks and limestones; 3) presence of tectonic displacement of host rocks and associated emplacement of dikes; 4) the presence of scattered pyrite and arsenopyrite; 5) mineralogical and geochemical profile of ores represented by sulfides and sulfosalts of Fe, Cu, Zn, Pb, As, Sb, Hg, and Tl; and 6) the ratio Au/Ag > 1 in gold-arsenic ores.

However, the Vorontsovskoe deposit has specific features which distinguishes it from Carlin-type deposits, namely: 1) spatial coincidence at the present erosional level of several types of gold mineralization related to different levels of development, temperature regime and time of formation; 2) low content of organic matter in ore and host rocks; 3) increased initial temperatures of formation of gold-arsenic ores (450 °C), which were responsible for quartz-sericite alteration, in addition to the termination of hydrothermal processes accompanied by near-surface overprinting weathering; 4) low As content in pyrite, which determines the ratio of isomorphic and native Au forms in this mineral; 5) prevalence of native gold as small particles enclosed in rock-forming minerals, rather than in pyrite; and 6) the presence of Mn minerals (alabandite, klerite, etc.), as well as isomorphic Mn in sphalerite and carbonates (up to 7 wt.% $MnCO_3$) due to the involvement of limestones containing this element (up to 0.2 wt.% $MnCO_3$) in ore-forming process.

In our tentative genetic model for the formation of the Vorontsovskoe deposit, Au-Hg-As mineralization is coeval with the Lower Devonian emplacement of the igneous rocks of the Auerbah volcano-plutonic complex. Water and carbon dioxide of the hydrothermal solutions most probably originated from magmas, whereas metamorphic water equilibrated with carbonate sedimentary rocks. Magma-related fluids dominated in the formation of skarns, jasperoids, and quartz veins in the Auerbah ore field, whereas metamorphic water prevailed during quartz-sericite hydrothermal alteration in volcano-sedimentary rocks and calcareous breccias. Bulk sulfur originated from the deep-seated magmas, which were crucial for the formation of skarn ore (type A1). During formation of other types of ores, juvenile sulfur mixed with that of sedimentary (type A2) or biogenic (types A3 and B1) sulfur. Gold and other ore components were introduced from the magmas during volcanic and intrusive activity and were also extracted from sedimentary rocks hosting the mineralization.

Acknowledgements

The present investigation was supported by state assignment projects of IGG UB RAS (themes 0393-2014-0022), IGM SB RAS (VIII.72.2.1.) and partially by RFBR grant 16-05-00353. We are grateful to the employees of the Geological Survey of “Northern Urals Gold” A.G. Ashikhnin and A.A. Gottman for allowing us to visit the Vorontsovskoe open pit mine.

Discussions and assistance in the study of organic matter from N.G. Petrishchev (Institute of Geology and Geochemistry, RAS, Urals Branch), O.V. Koryakova and M.I. Kodess (Institute of Organic Syntesis, RAS, Urals Branch), M. Yu. Yanchenko (Institute of Solid State Chemistry, RAS, Urals Branch), and N.N. Gusev (All-Russian Scientific-Research Institute of Mineral Resources, Moscow) are appreciated.

We would like to thank S.P. Glavatskikh (IGG UB RAS), S.V. Akulov (The Ural State Mining University), Y. Schegolkova and T.P. Zubkov (FSUE TsNIGRI, Moscow), who helped us to study the specific features of pyrite and to O. Yu. Plotinskaya (IGEM RAS, Moscow) and S. Tessalina (Curtin University, Australia) for valuable comments and help with editorial procedures.

References

Airiyants, E.V., Zhmodik, S.M., Mironov, A.G., Borovikov, A.A., 2007. Gold mineralization in siliceous-carbonate rocks of southeastern East Sayan. Russ. Geol. Geophys. 48, 389–399.

Alvarez, A.A., Noble, D.C., 1988. Sedimentary rock-hosted disseminated precious metal mineralization at Purisima Concepcion, Yauricocha District, Central Peru. Econ. Geol. 83, 1368–1378.

Anand, R.R., 2011. Weathering history, landscape evolution and implications for exploration. In: Butt, C.R.M., Cornelius, M., Scott, K.M., Robertson, I.D.M. (Eds.), Regolith Expression of Australian Ore Systems, CRC LEME Report, pp. 15–45.

Arehart, G.B., Donelick, R.A., 2006. Thermal and isotopic profiling of the Pipeline hydrothermal system: application to exploration for Carlin-type gold deposits. J. Geochem. Explor. 91, 27–40.

Arehart, G.B., Foland, K.A., Naeser, C.W., Kesler, S.E., 1993. $^{40}Ar/^{39}Ar$, K/Ar, and fission track geochronology of sediment-hosted disseminated gold deposits at Post/Betze, Carlin trend, northeastern Nevada. Econ. Geol. 88, 622–646.

Artemenko, V., Artemenko, O., 2002. The mineral composition of Carlin-type gold mineralization in carbonate rocks of the Southern Donbas. Proceedings of IV International Symposium “Mineralogical Museums”. SPb. NIIZK St. Petersburg State University, pp. 5–6 (in Russian).

Asadi, H.H., Voncken, J.H.L., Hale, M., 1999. Invisible gold at Zarshuran, Iran. Econ. Geol. 94, 1367–1374.

Asadi, H.H., Voncken, J.H.L., Kuhnel, R.A., Hale, M., 2000. Petrography, mineralogy and geochemistry of the Zarshuran Carlin-like gold deposit, Northwest Iran. Mineral. Deposita 35, 565–671.

Azovskova, O.B., Rovnushkin, M.Y., Kazakov, O.V., Yurchenko, M.Y., 2011. Organic matter in the ores and host rocks of Vorontsovskoe. Yearbook 2010, IGG UB RAS, pp. 46–51 (in Russian).

Azovskova, O.B., Barannikov, A.G., Smagin, I.V., Rovnushkin, M.U., 2013a. The polygenic nature of the oxidized ores Vorontsovskoe gold deposit. Proceedings of the Conference “Ore-forming Process: From Genetic Concepts to Forecast and the Discovery of New Ore Deposits and the Provinces”. IGEM RAS, Moscow, p. 120 (in Russian).

Azovskova, O.B., Malyugin, A.A., Nekrasova, A.A., Yanchenko, M.Y., 2013b. Pyrite from zones of Mz-Kz reactivation of large faults on the eastern slope of the Ural Mountains, Russia. WASET. Eng. Technol. 79, 463–467 (London).

Bagby, W.C., Berger, B.R., 1985. Geologic characteristics of sediment-hosted, disseminated precious-metal deposits in the western United States. In: Berger, B.R., Bethke, P.M. (Eds.), Geology and geochemistry of epithermal systems: Reviews in Economic Geology. v. 2, pp. 169–202.

Bakulin, Y.I., 1998. Deposits of a Nevadian - type fine-dispersed gold - a type of primary sedimentary deposits regeneration. Russ. J. Pac. Geol. 17 (4), 126–128.

Barannikov, A.G., Ugrumov, A.N., 2003. Problems of Mesozoic endogenous gold mineralisation of the Urals. Lithosphere 1, 13–26 (in Russian).

Begetnev, S.V., 1999. Gold-bearing jasperoids of Auerbah ore cluster and its importance for prospecting (Ph.D. thesis. Yekaterinburg. (in Russian)).

Berger, B.R., Bagbby, W.C., 1993. The geology and origin of Carlin-type gold deposits. In: Foster, R.P. (Ed.), Gold Metallogeny and Exploration 1993. Chapman & Hall, pp. 210–248.

Bezmen, N.I., Tikhomirov, V.I., Kosogorova, V.N., 1975. Pyrite, pyrrhotite geothermometer: distribution of nickel and cobalt. Geokhimiya 5, 700–714.

Bobrov, V.N., 1991. Metasomatic and accompanying gold zoning in the precious metals ore field. Ore-bearing metasomatic formations of the Urals. Ural Branch of the Academy of Sciences of the USSR, Sverdlovsk, pp. 44–46.

Bodnar, R.J., Vityk, M.O., 1994. Interpretation of microthermometric data for H_2O-NaCl fluid inclusions. Fluid inclusions in minerals: methods and applications. In: De Vivo, B., Frezzotti, M.L. (Eds.), Pontignano-Siena, pp. 117–130.

Borisenko, A.S., 1977. Cryometric analysis of salt composition in vapor-fluid inclusions in minerals. Geol. Geofiz. 8, 16–27.

Borisenko, A.S., Khoa, C.C., Izokh, A.E., Dashkevich, E.G., Nevolko, P.A., 2008. Mineralogical and geochemical peculiarities of ores and age of Au-As mineralization in the North Vietnam. In: Zaykov, V.V., et al. (Eds.), Metallogeny of Ancient and Modern Oceans. Ore-bearing Complexes and Ore facies, Scientific ed. IMinUB RAS, Miass, pp. 218–221 (in Russian).

Chekvaidze, V.B., Isaakovich, I.Z., Milyaeva, S.A., 1995. Mineralogical and geochemical criteria for prospecting gold-bearing regolith of North Urals. Ores Metals 5, 25–35 (in Russian).

Cheremisin, A.A., Zlotnik-Khotkevich, A.G., 1997. Vorontsovskoe gold deposit. Ores Metals 1, 59–70 (in Russian).

Chudnenko, K.V., Palyanova, G.A., Anisimova, G.S., Moskvitin, S.G., 2015. Physicochemical modeling of formation of Ag–Au–Hg solid solutions: Kyuchyus deposit (Yakutia, Russia) as an example. Appl. Geochem. 55, 138–151.

Cline, J.S., Hofstra, F.F., 2000. Ore-fluid evolution at the Getchell Carlin-type gold deposit, Nevada, USA. Eur. J. Mineral. 12 (1), 195–212.

Cline, J.S., Hofstra, A.H., Muntean, J.L., Tosdal, R.M., Hickey, K.A., 2005. Carlin-type gold deposits in Nevada: critical geologic characteristics and viable models. Society of Economic Geologists, Inc. Economic Geology 100th Anniversary Volume, pp. 451–484.

Çolakoğlu, A.R., Oruç, M., Arehart, G.B., Poulson, S., 2011. Geology and isotope geochemistry (C–O–S) of the Diyadin gold deposit, Eastern Turkey: a newly-discovered Carlin-like deposit. Ore Geol. Rev. 40, 27–40.

Crafford, A.E.J., Grauch, V.J.S., 2002. Geologic and geophysical evidence for the influence of deep crustal structures on Paleozoic tectonics and the alignment of world-class gold deposits, north-central Nevada, USA. Ore Geol. Rev. 21, 157–184.

Craig, J.R., Vaughan, D.J., 1981. Ore Microscopy and Ore Petrography. John Wiley and Sons, NewYork.

Craw, D., Upton, P., Horton, T., Williams, J., 2013. Migration of hydrothermal systems in an evolving collisional orogen, New Zealand. Mineral. Deposita 48, 233–248.

Cromie, P.W., Khin, Z., 2003. Geological setting, nature of ore fluids and sulphur isotope geochemistry of the Fu Ning carlin-type gold deposite, Yunnan Province, China. Geofluids 3, 133–143.

Einaudi, M.T., Meinert, L.D., Newberry, R.J., 1981. Skarn Deposits: Econ. Geol., 75th Anniv. Vol. pp. 317–391.

Emsbo, P., Hofstra, A.H., Lauha, E.A., Griffin, G.L., Hutchinson, R.W., 2003. Origin of high-grade gold ore, source of ore fluid components, and genesis of the Meikle and neighboring Carlin-type deposits, Northern Carlin Trend, Nevada. Econ. Geol. 98, 1069–1105.

Faure, G., 1986. Principles of Isotope Geology. second ed. Wiley, New York.

Fleck, R.J., Sutter, J.F., Elliot, D.H., 1977. Interpretation of discordant $^{40}Ar/^{39}Ar$ age spectra of Mesozoic tholeiites from Antarctica. Geochim. Cosmochim. Acta 41, 15–32.

Fleet, M.E., Mumin, A.H., 1997. Gold-bearing arsenian pyrite and marcasite and arsenopyrite from Carlin Trend gold deposits and laboratory synthesis. Am. Mineral. 82, 182–193.

Freyssinet, P., Butt, C.R.M., Morris, R.C., Piantone, P., 2005. Ore forming processes related to lateritic weathering. Economic Geology 100th Anniversary Volume, pp. 681–722.

Grabezhev, A.I., Ronkin Yu, L., Puchkov, V.N., Gerdes, A., Rovnushkin, M.Y., 2014. Krasnotur'insk skarn copper ore field, northern Urals: the U–Pb Age of ore-controlling diorites and their place in the regional metallogeny Dokl. Earth Sci. 456 (2), 641–645.

Grigor'ev, N.A., Sazonov, V.N., Murzin, V.V., Shorohov, G.P., 1992. Mineral balance of copper, silver and gold in metasomatites of skarn deposits of Turinsky group. Geokhimiya 9, 1353–1360.

Grinenko, V.A., 1962. Preparation of sulfur dioxide for isotopic analysis. J. Inorg. Chem. 7, 578–582 (in Russian).

Gromakovsky, I.Y., Stepanov, V.A., 1999. Gold mineralization in carbonate thick units of Oktyabrsky region, Priamurie. Russ. J. Pac. Geol. 18 (1), 84–90.

Groves, D.I., Goldfarb, R.J., Gebre-Mariam, M., Hagemann, S.G., Robert, F., 1998. Orogenic gold deposits: a proposed classification in the context of their crustal distribution and relationships to other gold deposit types. Ore Geol. Rev. 13, 7–27.

Gu, X.X., Liu, J.M., Schulz, O.F., Vavtar, M.H., Zheng, M.H., 2002. Syngenetic origin for the sediment-hosted disseminated gold deposits in NW Sichuan, China: ore fabric evidence. Ore Geol. Rev. 22, 91–116.
Gu, X.X., Zhang, Y.M., Li, B.H., Dong, S.Y., Xue, C.J., Fu, S.H., 2012. Hydrocarbon- and ore-bearing basinal fluids: a possible link between gold mineralization and hydrocarbon accumulation in the Youjiang basin, South China. Mineral. Deposita 47, 663–682.
Hausen, D.M., Kerr, P.E., 1968. Fine gold occurrence at Carlin, Nevada, in Ridge, J.D., ed., Ore deposits of the United States, 1933–1967 (Graton-Sales volume): New York. Am. Inst. Min. Metall. Eng. 1, 908–940.
Hazarika, P., Mishra, B., Chinnasamy, S.S., Bernhardt, H.-J., 2013. Multi-stage growth and invisible gold distribution in pyrite from the Kundarkocha sediment-hosted gold deposit, eastern India. Ore Geol. Rev. 55, 134–145.
Hofstra, A.H., 1994. Geology and genesis of the Carlin-type gold deposits in the Jerritt Canyon district, Nevada: Unpublished Ph.D. thesis, Boulder, Colorado, University of Colorado.
Hofstra, A.H., Cline, J.S., 2000. Characteristics and models for Carlin-type gold deposits. In: Hagemann, S.G., Brown, P.E. (Eds.), Gold in 2000. Reviews in Economic Geology 13, pp. 163–220.
Hu, R.-Z., Su, W.-C., Bi, X.-W., Tu, G.-Z., Hofstra, A.H., 2002. Geology and geochemistry of Carlin-type gold deposits in China. Mineral. Deposita 37, 378–392.
Ilchik, R.P., Barton, M.D., 1997. An amagmatic origin of Carlin-type gold deposits. Econ. Geol. 92, 269–288.
JORC, 2012. The JORC Code. 2012 ed. Australian Institute of Geoscientists, Australian Institute of Mining and Metallurgy, Mineral Council of Australia (44 pp.).
Kochneva, N.T., Volkov, A.V., Serafimovski, T., Tasev, G., Tomson, I.N., 2006. Tectonic position of the Alshar Au–As–Sb–Tl deposit, Macedonia. Geol. Ore Deposits 406 (6), 784–787.
Konstantinov, M.I., 2006. Gold Ore Province in the World. The scientific world, Moscow (in Russian).
Korzhinskiy, D.S., 1948. Petrology of Turinskiy Skarn Copper Deposits. Publishing House of the USSR Academy of Sciences, Moscow.
Kovalev, K.R., Kalinin, Y.A., Naumov, E.A., Pirajno, F., Borisenko, A.S., 2009. A mineralogical study of the Suzdal sediment-hosted gold deposit, Eastern Kazakhstan: implications for ore genesis. Ore Geol. Rev. 35, 186–205.
Krasnobaev, A.A., Fershtater, G.B., Bogomolov, E.S., et al., 2007. Auerbah granitoid massif: zircons, age, polichrono. Yearbook 2006 Institute of Geology and Geochemistry. Information Collection of Scientific Papers. IGG UB RAS, Yekaterinburg, pp. 191–196.
Kretschmar, U., Scott, S.D., 1976. Phase relations involving arsenopyrite in the system Fe-As-S and their application. Can. Mineral. 14, 364–386.
Kuzmina, O., Diachkov, B.A., Vladimirov, A.G., 2013. Main criteria and preconditions for the prospecting of gold deposits of jasperoid type (East Kazakhstan). Lithosphere 6, 54–64 (in Russian).
Large, R.R., Danyushevsky, L., Hollit, C., Maslennikov, V., Meffre, S., Gilbert, S., Bull, S., Scott, R., Emsbo, P., Thomas, H., Singh, B., Foster, J., 2009. Gold and trace element zonation in pyrite using a Laser Imaging techniqe: implications for the timing of gold in orogenic and Carlin-Style sediment-hosted deposits. Econ. Geol. 104, 635–668.
Lefebure, D.V., Brown, D.A., Ray, G.E., 1998. The British Columbia sediment-hosted gold project, in: British Columbia Geological Survey Branch. Geological Fieldwork. Paper 1999-1, pp. 165–178.
Lu, G.-Q., 1994. A genetic link between the gold-mercury mineralization and petroleum evolution - a case of the Danzhai gold-mercury deposit. A Thesis in Partial Fulfillment of the Requirements for the Degree of Doctor of Philosophy at l'Université du Québec à Chicoutimi, Chicoutimi, Québec, Canada, and the Institute of Geochemistry, the Chinese Academy of Sciences, Guiyang, Guizhou Province, P. R. China.
Maohong, C., Jingwen, M., Bierlein, F.P., Norman, T., Uttley, P.J., 2011. Structural features and metallogenesis of the Carlin-type Jinfeng (Lannigou) gold deposit, Guizhou Province, China. Ore Geol. Rev. 43, 217–234.
Mehrabi, B., Yardley, B.W.D., Komninue, A., 2003. Modelling the As-Au association in hydrothermal gold mineralization: example of Zarshuran deposit, NW Iran. J. Sci. Islam. Repub. Iran 14 (1), 37–52.
Minina, O.V., 1994. Auerbah complex ore-magmatic system in the Middle Urals. Otechestvennaya Geol. 7, 17–23 (in Russian).
Murzin, V.V., Sazonov, V.N., 1996. Mineral Assemblages and the Conditions for the Formation of Sulfide Gold Mineralisation at Turinsk-Auerbah Ore Cluster (Urals). Publishing House of Ural Branch of Russian Academy of Sciences, Yekaterinburg (in Russian).
Murzin, V.V., Sazonov, V.N., 1999. Gold-bearing mineral assemblages in the copper and iron skarn deposits of the Tur'insk-Ayerbakhovsk ore field and their formation condition (Urals, Russia). Geol. Ore Deposits 41 (4), 308–321.
Murzin, V.V., Bushmakin, A.F., Sustavov, S.G., Sherbachev, D.K., 1996. Clerite $MnSb_2S_4$ - a new mineral from the Vorontsovskoe gold deposit. Zapiski RMO (Proceedings of the Russian Mineralogical Society) 125, 3, pp. 106–112 (in Russian).
Murzin, V.V., Sazonov, V.N., Ronkin, Y.L., 2010. Model for formation of Vorontsovskoe gold deposit in the Urals (Carlin type): new data and problems. Lithosphere 6, 66–73 (in Russian).
Naumov, E.A., Gushchina, L.V., Borisenko, A.S., Borovikov, A.A., Babich, V.V., 2001. Conditions of forming of Hg-gold at the Au-Hg deposits. In: Piestrzynski, et al. (Eds.), Mineral Deposits at the Beginning of the 21st Century. Swets & Zeitlineger Publisher Lisse, pp. 867–870.
Naumov, E.A., Borovikov, A.A., Borisenko, A.S., Zadorozhniy, M.V., Murzin, V.V., 2002. Physicochemical conditions of formation of epithermal gold-mercury deposits. Geol. Geofiz. 43, 1003–1013.
Nechkin, G.S., Rovnushkin, M.U., 2011. Sulphide mineralization at the near-dikes areas at the Vorontsovskoe gold deposit (Auerbah complex, North Urals). Proceedings of the Institute of Geology and Geochemistry, Ural Branch of Russian Academy of Sciences. 158, pp. 187–190 (in Russian).
Nutt, C.J., Hofstra, A.H., 2003. Alligator Ridge District, East-Central Nevada: Carlin-type gold mineralization at shallow depths. Econ. Geol. 98, 1225–1241.
Ohmoto, H., Rye, R.O., 1979. Isotope of sulfur and carbon. In: Barnes, H.L. (Ed.), Geochemistry of Hydrothermal Deposits. John Wiley and Sons, pp. 509–567.
Ovchinnikov, L.N., 1948. Ores of Turinskiy Skarn Copper Deposits. UFAN USSR Sverdlovsk (in Russian).
Palenik, C.S., Utsunomiya, S., Reich, M., Kessler, S.E., Wang, L., Ewing, R.C., 2004. Invisible gold revealed: direct imaging of gold nanoparticles in a Carlin-type deposit. Am. Mineral. 89, 1359–1366.
Peters, S.G., Jiazhan, H., Zhiping, L., Chenggu, J., 2007. Sedimentary rock-hosted Au deposits of the Dian–Qian–Gui area, Guizhou, and Yunnan Provinces, and Guangxi District, China. Ore Geol. Rev. 31, 170–204.
Phillips, G.N., Powell, R., 1993. Link between gold provinces. Econ. Geol. 88, 1084–1098.
Pirajno, F., 2013. The Geology and Tectonic Settings of China's Mineral Deposits. Springer.
Radtke, A.S., 1985. Geology of the Carlin gold deposit, Nevada. U.S. Geol. Prof. Pap. N 1267.
Radtke, A.S., Scheiner, B.J., 1970. Studies of hydrothermal gold deposition (I). Carlin gold deposit, Nevada: the role of carbonaceous materials in gold deposition. Econ. Geol. 65, 87–102.
Radtke, A.S., Rye, R.O., Dickson, F.W., 1980. Geology and stable isotope studies of the Carlin gold deposit, Nevada. Econ. Geol. 75, 641–672.
Rakhov, E.V., 1999. The ore-bearing breccia of Vorontsovskoe deposit: structure, genesis And role in the formation of gold mineralization (Ph.D. thesis. Yekaterinburg. (in Russian)).
Reich, M., Kesler, S.E., Utsunomiya, S., Palenik, C.S., Chryssoulis, S.L., Ewing, R.C., 2005. Solubility of gold in arsenian pyrite. Geochim. Cosmochim. Acta 69, 2781–2796.
Ressel, M.W., Noble, D.C., Henry, C.D., Trudel, W.S., 2000. Dikehosted ores of the Beast deposit and importance of Eocene magmatism in gold mineralization of the Carlin trend, Nevada. Econ. Geol. 95, 1417–1444.
Rindzyunskaya, N.M., Polyakova, T.P., Bobrov, V.N., 1995. Geological and mineralogical characteristic of supergene zone of Vorontsovskoe gold deposit. Ore Metals 4, 42–52 (in Russian).
Ronkin, Y.L., Petrov, G.A., Lepikhina, O.P., 2009. Precision Sm-Nd isotope dating of Auerbah gabbro-granite complex (Northern Urals). Isotopic Systems and Time of Geological Processes. Proceedings of IV Russian Conference on Isotope Geochronology. vol. II, pp. 122–124 (St. Petersburg, (in Russian)).
Rovnushkin, M.Y., Azovskova, O.B., 2012. Organic matter in brecciated ores of Vorontsovskoe gold deposit, Urals. Metallogeny of ancient and modern oceans. Yimin UB RAS, Miass, pp. 190–194 (in Russian).
Rovnushkin, M.Y., Gulyaev, T.Y., Galakhova, O.L., 2010. K-feldspar metasomatism occurrence within Vorontsovskoe gold deposit. Proceedings of the IGG UB RAS. 157, pp. 241–244 (in Russian).
Savelyeva, K.P., Kostromin, D.A., 1991. Polygenic and polichrono metasomatismat the one of the gold deposits in the Northern Urals. Geol. metamorphic complexes. Ural.gorn. Inst, Yekaterinburg, pp. 75–80 (in Russian).
Sawkins, P.J., 1984. Metal Deposits in Relation to Plate Tectonics. Springer-Verlag, New York.
Sazonov, V.N., 1998. Gold bearing metasomatic formations of mobile belts. Ural Mining and Geological Academy, Yekaterinburg (in Russian).
Sazonov, V.N., Murzin, V.V., Grigoryev, N.A., Gladkovsky, B.A., 1991. Endogenous Mineralization of Devonian Andesite Volcano-plutonic Complex (Urals). Ural Branch of the Academy of Sciences of the USSR, Sverdlovsk (in Russian).
Sazonov, V.N., Murzin, V.V., Grigor'ev, N.A., 1998. Vorontsovskoe gold deposit: an example of Carlin-type mineralization in the Urals, Russia. Geol. Ore Deposits 40 (2), 139–151.
Seedorff, E., 1991. In: Raines, G.L., Lisle, R.E. (Eds.), Magmatism, Extension, and Ore Deposits of Eocene to Holocene Age in the Great Basin: Mutual Effects and Preliminary Proposed Genetic Relationships.
Sharp, Z.D., Essene, E.J., Kelly, W.C., 1985. A re-examination of the arsenopyrite geothrmometer: pressure considerations and applications to natural assemblages. Can. Mineral. 23, 517–534.
Shui, H.M., 1991. Occurence and distribution of invisible gold in a Carlin-type gold deposit in China. Am. Miner. 76, 1964–1972.
Sidorov, A.A., Volkov, A.V., 1998. Some structural and compositional similarities between the Carlin (Nevada, United States) and Maiskoe (Chukot Peninsula, Russia) gold–sulfide deposits. Dokl. Earth Sci. 359 (2), 236–241.
Sigov, A.P., 1969. Metallogeny of Mesozoic and Cenozoic in Urals. Nedra, Moscow (in Russian).
Sillitoe, R.H., Bonham Jr., H.F., 1990. Sediment-hosted gold deposits: distal products of magmatic-hydrothermal systems. Geology 18, 157–161.
Simon, G., Kesler, S.E., Chryssoulis, S.L., 1999. Geochemistry and texture of gold-bearing arsenian pyrite Twin Creeks, Nevada: implications for deposition of gold in the Carlin-type deposits. Econ. Geol. 94, 405–422.
Stepanov, V.A., 2000. Geology of gold, silver and mercury. Part 2. Gold and Mercury of Amur Province. Dalnauka, Vladivostok (in Russian).
Su, W., Xia, B., Zhang, H., Zhang, X., Hu, R., 2008. Visible gold in arsenian pyrite at the Shuiyindong Carlin-type gold deposit, Guizhou, China: implications for the environment and processes of ore formation. Ore Geol. Rev. 33, 667–679.
Su, W., Heinrich, C.A., Pettke, T., Zhang, X., Hu, R., Xia, B., 2009. Sediment-hosted gold deposits in Guizhou, China: products of wall-rock sulfidation by deep crustal fluids. Econ. Geol. 104, 73–93.
Talantsev, A.S., 1981. Geothermobarometry of Dolomite-Palcite Assemblages. Science, Moscow (in Russian).
Tauson, V.L., Babkin, D.N., Pastushkova, T.M., Krasnoshchekova, T.S., Lustenberg, E.E., Belozerova, O.Y., 2011. Dualistic distribution coefficients of elements in the system mineral–hydrothermal solution. I. Gold accumulation in pyrite. Geochem. Int. 49 (6), 568–578.

Taylor, G., Eggleton, R.A., 2001. Regolith Geology and Geomorphology. John Wiley and Sons, NewYork.
Tulmin, P., Barton, P.B., 1968. Thermodynamic investigation of pyrite and pyrrhotite. Thermodynamics of Post-magmatic Processes. Mir, Moscow, pp. 182–230 (in Russian).
Ugriumov, A.N., 1993. Jasperoid gold deposits (geology, regularities of localization and formation conditions) (Ph.D. thesis, Yekaterinburg. (in Russian)).
Velivetskaya, T.A., Ignatiev, A.V., Gorbarenko, S.A., 2009. Carbon and oxygen isotope microanalysis of carbonate. Rapid Commun. Mass Spectrom. 23, 2391–2397.
Volkov, A.V., Goncharov, V.I., Sidorov, A.A., 2006a. Gold and silver deposits in Chukotka. IGEM; Magadan NEISRI FEB RAS, Moscow.
Volkov, A.V., Serafimovski, T., Kochneva, N.T., Tomson, I.N., Tasev, G., 2006b. The Alshar epithermal Au–As–Sb–Tl deposit, Southern Macedonia. Geol. Ore Deposits 48 (3), 175–193.
Volkova, I.B., 1990. Organic Petrology. Nedra, Leningrad.
Wallace, A.R., 1989. The Relief Canyon Gold Deposit, Nevada: a mineralized solution breccia. Econ. Geol. 84, 279–290.
Wells, J.D., Mullens, T.E., 1973. Gold-bearing arsenian pyrite determined by microprobe analysis, Cortez and Carlin gold mines, Nevada. Econ. Geol. 68, 187–201.
Xia, Y., Su, W., Zhang, X., Liu, J., 2012. Geochemistry and metallogenic model of Carlin-type gold deposits in Southwest Guizhou Province, China. In: Panagiotaras, D. (Ed.), Geochemistry - Earth's System Processes. InTech, Shanghai, pp. 127–156.
Yazeva, R.G., Puchkov, V.N., Bochkarev, V.V., 1988. Complexes of active continental margin in Urals. Rep. USSR Acad. Sci. 300 (4), 927–931 (in Russian).
Ye, Z., Kesler, S.E., Essene, E.J., Zohar, P.B., Borhauer, J.L., 2003. Relation of Carlin-type gold mineralization to lithology, structure and alteration: Screamer zone, Betze-Post deposit, Nevada. Mineral. Deposita 38, 22–38.
Zheng, Y.F., 1993. Calculation of oxygen isotope fractionation in anhydrous silicate minerals. Geochim. Cosmochim. Acta 57, 1079–1091.
Zheng, Y.F., 1999. Oxygen isotope fractionation in carbonate and sulfate minerals. Geochem. J. 33, 109–126.
Zubkov, V.S., 2000. Endogenous ore deposit and naphtides. Geochemical processes and minerals. GeoIGU Bull. 2, 74–93 (in Russian).